

# Momentum-dependence in the infinitesimal Wilsonian renormalization group

**Moritz Helias**

Institute of Neuroscience and Medicine (INM-6) and Institute for Advanced  
Simulation (IAS-6) and JARA BRAIN Institute I, Jülich Research Centre,  
Jülich, Germany  
Department of Physics, Faculty 1, RWTH Aachen University, Aachen, Germany

**Abstract.** Wilson's original formulation of the renormalization group is perturbative in nature. We here present an alternative derivation of the infinitesimal momentum shell RG, akin to the Wegner and Houghton scheme, that is a priori exact. We show that the momentum-dependence of vertices is key to obtain a diagrammatic framework that has the same one-loop structure as the vertex expansion of the Wetterich equation. Momentum dependence leads to a delayed functional differential equation in the cutoff parameter. Approximations are then made at two points: truncation of the vertex expansion and approximating the functional form of the momentum dependence by a momentum-scale expansion. We exemplify the method on the scalar  $\varphi^4$ -theory, computing analytically the Wilson-Fisher fixed point, its anomalous dimension  $\eta(d)$  and the critical exponent  $\nu(d)$  non-perturbatively in  $d \in [3, 4]$  dimensions. The results are in reasonable agreement with the known values, despite the simplicity of the method.

## 1. Introduction

The renormalization group (RG) is a standard tool to study phase transitions in statistical physics as well as to investigate renormalizable field theories in high energy physics. Its field-theoretical formulation has initially been applied to renormalizable theories only [1]; those, in which all physical quantities can be expressed in terms of a few renormalized parameters. One here exploits the arbitrariness of the chosen scale at which the renormalized parameters are fixed to derive a differential equation in this scale parameter [2, 3, 4]. It was realized later that the field-theoretical formulation is also applicable to non-renormalizable theories [5]. Recent examples of non-renormalizable models describe erosion of landscapes [6, 7]. These models are structurally similar to a variant of the KPZ equation [8], the model by [9], whose RG flow was first shown by Antonov and Vasiliev to require arbitrary many couplings [10].

Conceptually quite different is the idea of Wilson's renormalization group, which studies how the action that describes a theory changes as short-ranged degrees of freedom are marginalized out. The interpretation is thus more intuitive. Initially, this scheme has been presented as an iterative method, where in each step a fixed fraction of the the momentum space is integrated out [11, 12]. A hard cutoff separates the marginalized, short-distance modes from the long-distance modes that remain after the marginalization step. One studies how the action evolves as the cutoff is lowered. This approach has the merit of a clear interpretation as a systematic coarse-graining. Also, the procedure is applicable to theories that originally possess a high momentum cutoff. Those appear, for example, in condensed matter problems, where the lattice spacing limits the magnitude of all momenta. The Wilsonian RG, too, is applicable also to non-renormalizable theories.

The classical computation in the Wilsonian RG, however, relies on a diagrammatic perturbation expansion. For this reason it is tied to the computation of properties of systems close to their upper critical dimension  $d_c$ , the dimensionality above which non-Gaussian terms can be neglected. In the vicinity below  $d_c$ , interaction vertices are small, presenting a natural expansion parameter. The  $\epsilon$ -expansion, operating in  $d_c - \epsilon$  dimensions, exploits this fact. Quantities of interest must ultimately be computed from typically divergent series in  $\epsilon$ , requiring appropriate resummation. Also, computations become complicated beyond one loop order due to the presence of the cutoff. In practice, one therefore often resorts to the field-theoretical formulation, even in the context of condensed matter problems.

Early on, Wegner and Houghton [13] presented a continuous version of the Wilsonian RG by employing a sharp cutoff and by marginalizing only over an infinitesimally thin momentum shell. But the simplicity of the diagrammatic formulation by Wilson was lost to some extent due to the employed projector formalism. The authors noted difficulties of a sharp cutoff: it generates a non-analytical momentum dependence of the vertices at vanishing momenta, which correspond to long-range interactions [11, p. 153]. This general problem of treating the momentum dependence within the Wilsonian RG has been noted early on [11, cf. Fig 11.1 and surrounding text]. A sharp cutoff is, however, needed ensure that the action maintains its rescaling invariance, the independence of physical results under the transform  $\varphi \rightarrow z\varphi$  [14]. This property must be kept in order to compute the anomalous dimension.

Morris [14] showed that there is in fact no fundamental problem of using a hard cutoff, if combined with the flow equation for the effective action [15], the Legendre

transformed Helmholtz free energy. A momentum-scale expansion can be made for the flow equation, where the momentum scale  $|k|$  is used as the expansion parameter. However, the author pointed out a conceptual problem: despite being an expansion for small external momenta, vertices evaluated at momenta as large as the cutoff are required to close the equations. Also, critical exponents turned out to be not as accurate as obtained with methods of comparable complexity. Kopietz [16] showed that the exact Wetterich flow equation for the effective action [15] indeed can be used to systematically derive results beyond one-loop order. A drawback of this method is the requirement to compute diagrams with more than a single loop.

The generality of the Wilsonian RG, working for renormalizable as well as for non-renormalizable theories, as well as its intuitive interpretation in terms of coarse-graining and its efficient diagrammatic formulation are desirable features. However, it has been pointed out that a momentum-scale expansion was incompatible with the closely related Wegner and Houghton RG equation, because the latter contained tree-diagrams besides one-particle irreducible components. The reason is that tree diagrams vanish only for zero external momenta, as the momentum on the connecting propagator is constrained to reside above the cutoff.

The main motivation of this work is three-fold: First, to clarify where approximations are made when studying the a-priori exact formulation of the infinitesimal Wilsonian momentum-shell RG. Second, to derive a tower of diagrammatic expressions that is logically consistent with the idea of a systematic coarse-graining and a hard cutoff between marginalized and non-marginalized modes. Third, to recheck if a momentum-scale expansion is compatible with this framework. The latter question arises because it seems unintuitive that there was a qualitative difference between the Wegner-Houghton and the Wetterich equation with a hard cutoff, as sometimes stated in the literature.

To this end we show that in fact a continuous Wilsonian RG equation with sharp cutoff can be derived naturally without the projector formalism by Wegner and Houghton and be interpreted diagrammatically. Our derivation in particular shows that there is no approximation implied by going to only a single loop. We find that again tree diagrams appear, but their treatment is actually quite simple: one can systematically keep only those tree diagrams that are needed to integrate the remainder of the flow equation that is composed of individual vertices with a single pair of legs contracted. This leads to a delayed functional differential equation in the cutoff parameter, where the delays depend on the external momenta. The structure of the resulting diagrams is in fact identical to those of the Wetterich equation. Tree diagrams disappear from the final effective long-range theory, as one evaluates all quantities on the long-distance scale of small momenta.

To perform actual computations, however, one is still forced to apply approximations, similarly as in the case of the Wetterich equation. We here employ two approximations to arrive at closed-form results: First, a truncation in the power of the field, only keeping a limited number of vertices for which we compute the flow. This approximation is naturally guided by the relevance of each term as indicated by its engineering dimension. Second, the momentum-dependence of the vertices is approximated in a momentum-scale approximation, as introduced by Morris [14] and employed in the context of the functional RG [17, 18].

We exemplify this method by computing an approximation of the critical exponent  $\nu$  and the anomalous dimension  $\eta$  of the scalar  $\varphi^4$ -theory. The computation requires only elementary spherically symmetric and uniaxial one-loop integrals. We show that

the flow equations can be evaluated far off the upper critical dimension  $d_c = 4$ , directly obtaining results for any dimension  $d \in [3, 4]$ . This demonstrates the non-perturbative nature of the equation. We find that the approximation for the critical exponent  $\eta$  is in between the values for the  $\epsilon$ -expansion of orders  $\epsilon^2$  and  $\epsilon^3$  and slightly better than the result obtained by Morris [14]. It is, moreover, far better than the second order  $\epsilon$ -expansion, despite only requiring one-loop integrals. Also there is no divergent series to be resummed to obtain estimates for critical exponents.

The results in Section 2 are presented in a self-contained manner. The initial sections set up the notation and present a coherent exposure of the basic idea of the renormalization group: In Section 2.1 we introduce the notation for the field theory to be considered and the  $\varphi^4$ -theory as a particular example. Section 2.2 defines the procedure of coarse-graining in Fourier domain. Section 2.3 derives an exact flow equation for the coarse-grained action. Section 2.4 motivates the comparison between the Wetterich and the Wegner-Houghton scheme. Section 2.5 discusses the two distinct classes of graphs, single loops and trees, that contribute and shows how they are combined to obtain one-loop diagrams of identical structure as those of the Wetterich equation. It shows how the momentum dependence of effective vertices couples different decimation steps in the flow equation. Section 2.6 derives concrete expressions for these diagrams. Rescaling of momenta and fields, required to obtain fixed points, is the topic of Section 2.7.

The method is then illustrated on the example of the  $\varphi^4$ -theory, obtaining a general expression for the momentum dependence of the four-point vertex in Section 2.8, which is reduced to a set of coupled differential equations for the interaction in Section 2.9 and for the self-energy in Section 2.10. Section 2.11 determines the fixed points in dimensions  $d \in [3, 4]$  and computes the critical exponents  $\nu(d)$  and  $\eta(d)$ . Section 3 summarizes the results in the light of the literature and compares this interpretation of the Wilsonian RG to the  $\epsilon$ -expansion [11, 12] and to the work by Wegner & Houghton [13].

## 2. Results

We here chose a notation that should be easy to transfer to other problems. For concreteness, we here choose the language of classical statistical field theory, in particular to bosonic fields. In the following Section 2.1 we set up the language and define elementary quantities.

### 2.1. Model system

We assume a form of the action

$$S[\varphi] = -\frac{1}{2} \varphi^T G^{-1} \varphi, \quad (1)$$

$$+ \sum_{n=3}^{\infty} \frac{1}{n!} \int_{k_1} \cdots \int_{k_n} S^{(n)}(k_1, \dots, k_n) \varphi(k_1) \cdots \varphi(k_n),$$

of a translation-invariant system, so that the quadratic part  $G^{-1} \equiv -S^{(2)}$  and the bare interaction vertices  $S^{(n)}$  all conserve momenta

$$G^{-1}(k_1, k_2) \propto \delta(k_1 + k_2), \quad (2)$$

$$S^{(n)}(k_1, \dots, k_n) \propto \delta(k_1 + \dots + k_n).$$

As a particular example, we study the  $\varphi^4$ -theory

$$S[\varphi] = -\frac{1}{2} \int_k \varphi(-k) (r^{(0)} + r^{(2)} k^2) \varphi(k) - u^{(0)} \int_{k_1} \int_{k_2} \int_{k_3} \varphi(k_1) \varphi(k_2) \varphi(k_3) \varphi(-k_1 - k_2 - k_3), \quad (3)$$

as a prototypical system, for which the Gaussian part  $G^{-1}$  is given by  $r^{(0)} + r^{(2)} k^2$  and there is only a single bare interaction vertex  $u^{(0)} \delta(k_1 + \dots + k_4)$ . The superscripts here refer to the order in  $k$  of the momentum dependence. A configuration of the field  $\varphi(k)$  is realized with probability of Boltzmann form

$$p[\varphi] \propto \exp(S[\varphi]),$$

and the system is described by the partition function

$$\mathcal{Z} = \int D\varphi \exp(S[\varphi]). \quad (4)$$

## 2.2. Definition of coarse-graining

We assume the system lives on a space  $r \in \mathbb{R}^d$  and the elementary entities (e.g. spins) have a lattice spacing  $a$ . Correspondingly, we have a high-momentum cutoff  $\Lambda = \frac{\pi}{a}$ , so that  $|k| < \Lambda$ .

We use the notation  $\varphi_{<}$  for the coarse-grained field that is defined in terms of the long-ranged degrees of freedom

$$\varphi_{<}(r) := \int_{0 \leq |q| < \Lambda_\ell} \varphi(q) e^{iqr}, \quad (5)$$

where we only take the Fourier integral up to the new cutoff  $\Lambda_\ell := \Lambda/\ell$  with an  $\ell > 1$ . Here and in the following we use the short hand  $\int_{0 \leq |q| < \Lambda_\ell} = \int_{0 \leq |q| < \Lambda_\ell} \frac{d^d q}{(2\pi)^d}$ . Analogously we define the short-ranged degrees of freedom as

$$\varphi_{>}(r) := \int_{\Lambda_\ell < |k| < \Lambda} \varphi(k) e^{ikr}.$$

Here and in the following we will denote momenta as  $q$  if they are long-ranged,  $0 < |q| < \Lambda_\ell$ , and those as  $k$  which short ranged,  $\Lambda_\ell < |k| < \Lambda$ .

The Fourier transform decomposes the fluctuations into long-ranged  $\varphi_{<}$  and short-ranged  $\varphi_{>}$  ones; with the linearity of the Fourier transform and the orthogonality of Fourier modes, it yields a decomposition of the entire field into the direct sum

$$\varphi = \varphi_{<} + \varphi_{>}.$$

We may ask which action  $S_\ell$  effectively controls the coarse-grained modes  $\varphi_{<}$ . This question reduces to a marginalization of the fast modes and we define the action for the slow modes as

$$\exp(S_\ell[\varphi_{<}]) := \int \mathcal{D}\varphi_{>} \exp(S[\varphi_{<} + \varphi_{>}]), \quad (6)$$

where the notation  $\int \mathcal{D}\varphi_{>}$  should be read as the integral of all Fourier modes with  $\Lambda_\ell < |k| < \Lambda$ . We call this step decimation. By this definition and the orthogonality of Fourier modes we have

$$\int \mathcal{D}\varphi = \int \mathcal{D}\varphi_{<} \int \mathcal{D}\varphi_{>}$$

so that the partition function (4) can be written in terms of the coarse-grained action alone

$$\mathcal{Z} = \int \mathcal{D}\varphi_{<} \exp(S_\ell[\varphi_{<}]).$$

Performing the marginalization over a finite momentum shell, the modes with Fourier coefficients  $|k| \in [\Lambda_\ell, \Lambda]$  are integrated out. After this step, the range of momenta is limited to  $0 < |q| < \Lambda_\ell$ .

To find a fixed point we need to bring the action into a comparable form as the initial action, thus rescaling the length scale by  $\ell$  and the momentum scale correspondingly as

$$\ell q =: k_\ell, \quad (7)$$

so that there are two consecutive steps

$$S[\varphi(k)]_{|k| \in [0, \Lambda]} \xrightarrow{\text{decimation}} S_\ell[\varphi_{<}(q)]_{|q| \in [0, \Lambda_\ell]} \xrightarrow{\text{rescaling}} S_\ell[\varphi_\ell(k_\ell)]_{|k_\ell| = |\ell q| \in [0, \Lambda]} . \quad (8)$$

### 2.3. The exact flow equation

The aim of this section is to derive a differential form for the Wilson RG. To this end, we consider the difference between the coarse-grained action  $S_{\ell \cdot (1+\delta)}$ , defined as (6), and the action  $S_\ell$ ; the cutoff  $\Lambda_\ell$  is thus lowered by an infinitesimal amount controlled by  $\delta > 0$ . The assumption is thus that all modes  $|k| > \Lambda_\ell$  have been marginalized and we integrate over the next lower interval of modes

$$\Lambda_{\ell \cdot (1+\delta)} \equiv \frac{\Lambda_\ell}{1+\delta} < |k| < \Lambda_\ell. \quad (9)$$

To obtain a flow equation, consider the difference between the coarse-grained action (6) after this marginalization step and before

$$\begin{aligned} S_{\ell \cdot (1+\delta)}[\varphi_{<}] - S_\ell[\varphi_{<}] &= \ln \left( \int \mathcal{D}\varphi_{>} \exp(S_\ell[\varphi_{<} + \varphi_{>}]) \right) \\ &\quad - S_\ell[\varphi_{<}] \\ &= \ln \int \mathcal{D}\varphi_{>} \exp(S_\ell[\varphi_{<} + \varphi_{>}] - S_\ell[\varphi_{<}]). \end{aligned} \quad (10)$$

The logarithm appearing on the right hand side, by the linked cluster theorem (see e.g. [3] or [19, Appendix A.3]), ensures that only connected diagrams need to be taken into account. The integrand can be expanded as

$$\begin{aligned} S_\ell[\varphi_{<} + \varphi_{>}] - S_\ell[\varphi_{<}] &= \varphi_{>}^T S_\ell^{(1)}[\varphi_{<}] + \frac{1}{2} \varphi_{>}^T S_\ell^{(2)}[\varphi_{<}] \varphi_{>} \\ &\quad + \mathcal{O}(\varphi_{>}^3), \end{aligned} \quad (11)$$

where  $S_{\ell,k}^{(1)} \equiv \frac{\delta S_\ell}{\delta \varphi(k)}$  and  $S_{\ell,-k,k}^{(2)} = \frac{\delta^2 S_\ell}{\delta \varphi(-k) \delta \varphi(k)}$  denote the first and second functional derivatives of the action. The first line in (11) leads to a Gaussian integral in (10). Now, each integration over  $\varphi_{>}$  has a momentum constrained to the shell  $\Lambda_{\ell \cdot (1+\delta)} < |k| < \Lambda_\ell$  and thus contributes in proportion to the integrated volume in  $k$ -space, which is  $\propto \delta$ , the thickness of the momentum shell.

Taking the limit  $\delta \rightarrow 0$  and considering only the infinitesimal change of the action on the left hand side of (10) as

$$\lim_{\delta \rightarrow 0} \frac{1}{\delta} (S_{\ell \cdot (1+\delta)} - S_\ell) \equiv \ell \frac{dS_\ell}{d\ell}, \quad (12)$$

all diagrams generated by the terms  $\mathcal{O}(\varphi_{>}^3)$  are  $\mathcal{O}(\delta^2)$ , because they need at least two propagators and thus two independent momentum integrals to contract all  $\varphi_{>}$  fields; these terms therefore vanish in the considered limit. As a result, only the Gaussian integral involving the first line of (11) remains, leading to

$$\begin{aligned} \ell \frac{dS_\ell}{d\ell} [\varphi_{<}] &= \frac{1}{2} \int_{|k|=\Lambda_\ell} \ln (G_{\ell, -k, k}[\varphi_{<}]) \\ &+ \frac{1}{2} \int_{|k|=\Lambda_\ell} S_{\ell, -k}^{(1)}[\varphi_{<}] G_{\ell, -k, k}[\varphi_{<}] S_{\ell, k}^{(1)}[\varphi_{<}], \end{aligned} \quad (13)$$

where we defined the propagator  $G_{\ell, -k, k}[\varphi_{<}] := (-S_{\ell, -k, k}^{(2)}[\varphi_{<}])^{-1}$ . The first line results from the normalization term of the Gaussian integral  $-\frac{1}{2} \ln \prod_{|k|=\Lambda_\ell} (-S_{\ell, -k, k}^{(2)}[\varphi_{<}])$ . This equation is an exact flow equation for the coarse-grained action  $S_\ell$ . Apart from a different derivation and notation, this equation is identical to the Wegner-Houghton equation [13, their eq. (2.14)].

#### 2.4. Relation to the Wetterich equation

What is the relation to the Wetterich equation ([15], for a review see [20, eq. 2.19])? The latter being an exact flow equation that is of one-loop structure. Both are functional differential equations: The Wetterich equation for the effective action  $\Gamma$ , the first Legendre transform of the free energy  $\ln \mathcal{Z}$ ; the Wegner-Houghton equation (13) for the Wilson effective action  $S_\ell$  defined by (6). In particular it may, at first sight, be surprising why eq. (13) contains two terms, while in the Wetterich equation only a single term appears that produces diagrams with a single closed loop. This apparent difference in the structure of the equations can be resolved by considering the dependence on external momenta of the vertices  $S_\ell^{(n)}$ , as shown in the following.

#### 2.5. Two classes of graphs: single loops and trees

Expanding the action into vertices (1), written for short as  $S_\ell[\varphi] = \sum_n S_\ell^{(n)} \varphi^n / n!$ , the exact flow equation (13) has two contributions:

*Single loops* The first line of (13) has a one-loop structure that becomes apparent when considering functional derivatives by  $\varphi$ ; the first derivative by  $\varphi(q)$ , for example, yields a tadpole contribution

$$\frac{1}{2} \int_{|k|=\Lambda_\ell} S_{\ell, -k, q, k}^{(3)} G_{\ell, k, -k} \equiv 3 \cdot \text{tadpole diagram},$$

which looks like a usual one-loop correction to the equation of state. Taking further derivatives by  $\varphi$ , the first line of (13) produces the usual structure of one-loop

diagrams. Considering the second functional derivative by  $\varphi(q)$  and  $\varphi(-q)$ , with  $\delta/\delta\varphi(-q) G_{\ell,k,-k} = G_{\ell,k,-k} S_{\ell,-k,-q,k}^{(3)} G_{\ell,k,-k}$ , one obtains

$$\begin{aligned} & \frac{1}{2} \int_{|k|=\Lambda_\ell} S_{\ell,-k,q,-q,k}^{(4)} G_{\ell,k,-k} \\ & + \frac{1}{2} \int_{|k|=\Lambda_\ell} S_{\ell,-k,q,k}^{(3)} G_{\ell,k,-k} S_{\ell,-k,-q,k}^{(3)} G_{\ell,k,-k}. \end{aligned} \quad (14)$$

Compared to the usual loopwise expansion [3, 4] (see [21] Chapter XIV for a presentation in the same notation), there are, however, three differences:

- the propagator  $G_\ell \equiv (-S_\ell^{(2)})^{-1}$  and the vertices  $S_\ell^{(n)}$ , being solutions of the differential equation (13), contain all fluctuation corrections from the scales  $\Lambda_\ell < |k| < \Lambda$  that have already been integrated out;
- the momentum integration is constrained to a single shell  $\int_{|k|=\Lambda_\ell}$ ;
- all propagator lines carry exactly the same momentum  $k$ .

These points hold in general also for higher derivatives. The last point has implications for the dependence on external momenta: the second line of (14) contributes only at vanishing external momentum  $q = 0$  by the assumption of a theory with momentum-conserving vertices  $S_{-k,-q,k}^{(3)} \propto \delta(q)$  (cf. (2)). The first line contributes to potentially all external momenta  $q$ .

The structure of the first diagram is a single vertex with two of its legs contracted by a propagator. Such one loop diagrams have a non-trivial flow equation, in the sense that multiple decimation steps  $\ell$  contribute to a vertex at a given and fixed set of external momenta. To see this explicitly, we take as an example a portion of the one-loop integral



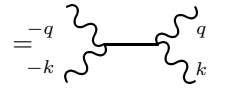
$$(15)$$

where the wiggly lines denote amputated legs and the full lines the connection points of a propagator. Now consider the point  $q_1 = -q_2$  in momentum space that obeys momentum conservation of the amputated legs. The full lines can then be closed by a propagator  $G_\ell(k)$ . By momentum conservation at the vertex, any value of  $k$  is allowed. So all decimation steps  $\ell$ , where a momentum shell  $|k| = \Lambda_\ell$  is marginalized, will contribute to the flow of the vertex function at this set of external momenta.

*Trees* The second line of (13) comprises two components  $S_{\ell'}^{(1)}$  that are connected by a single propagator  $G_{\ell'}$ , which we call reducible diagrams. These diagrams therefore have tree topology. Expanded in vertices  $S_{\ell'}^{(n)}$ , this contribution is the sum of pairs of vertices connected by a single line. The first derivative  $\delta/\delta\varphi_{>}$  in  $S_{\ell'}^{(1)}$  produces the usual combinatorial factor  $n$  for each term  $S_{\ell'}^{(n)} \varphi_{>}^n / n!$  of the expansion. The flow equation of these tree diagrams is trivial in the sense that only a single decimation step contributes to each tree: The decimation step  $\ell'$  of the momentum shell that contains the momentum  $k'$  of the connecting propagator  $G_{\ell'}(k')$ , which is  $|k'| = \Lambda_{\ell'}$ .



As an example consider the tree diagram

$$\frac{1}{2} \int_{k,q} \frac{\varphi(-k) \varphi(-q)}{2!} S_{\ell', -k, -q, k'}^{(3)} G_{\ell', k', -k'} S_{\ell', -k', q, k}^{(3)} \frac{\varphi(k) \varphi(q)}{2!} \quad (16)$$


The resulting contribution is an effective four-point vertex  $S_{\ell'}^{(4)}$  with external momenta  $-q, -k, q, k$ . The external momenta  $(k, q)$  uniquely determine the momentum  $k' = k+q$  of the connecting propagator and thus the decimation step  $\ell'$  by  $|k'| = \Lambda_{\ell'} \equiv \Lambda/\ell'$ . For the diagram to exist in the effective action  $S_{\ell}$ , the corresponding shell must have been integrated, so  $\ell \geq \ell'$ . In summary,

- contributions from tree diagrams to the coarse-grained action can be integrated trivially; they have a non-vanishing value whenever the momentum  $k'$  of the propagator that connects the pair of vertices of the tree is not below the current cutoff  $|k'| \geq \Lambda_{\ell}$ ;
- as a consequence, the decimation step  $\ell'$  within which a tree diagram is created depends on the momentum  $k'$  as  $|k'| = \Lambda_{\ell'} \equiv \Lambda/\ell'$ .

*Combining loops and trees* Because only a single decimation step contributes to each tree, when integrating the flow equation (13), tree diagrams can directly be substituted in place of the effective vertices. This allows the construction of composed diagrams, illustrated in Figure 2: In a first decimation step at scale  $\ell'$ , a tree diagram (16) is produced, creating an effective four point vertex  $S_{\ell'}^{(4)}$ . At scale  $\ell > \ell'$ , the first line of (14) contracts its two legs with momenta  $k$  and  $-k$  with the propagator  $G_{\ell, k, -k}$  to form a single loop, resulting in

$$\frac{1}{2} \int_{|k'| > \Lambda_{\ell}} \int_{|k| = \Lambda_{\ell}} S_{\ell'(k'), -k', q, k}^{(3)} G_{\ell, k, -k} S_{\ell'(k'), -k, -q, k'}^{(3)} G_{\ell'(k'), k', -k'}. \quad (17)$$

The structure and combinatorial factor is hence the same as the second line of (14), only that it is non-vanishing also for  $q \neq 0$ . The resulting diagrams in general have the following properties:

- they have the one-loop structure known from the loopwise fluctuation expansion;
- at decimation step  $\ell$  there is precisely one single-scale propagator, a propagator whose momentum is constrained to the shell of the current decimation step,  $G_{\ell}(k)$  with  $|k| = \Lambda_{\ell}$ ;
- all other propagators  $G_{\ell'}$  belong to scales  $\ell' < \ell$  that have already been integrated out, so they carry momenta  $|k'| > \Lambda_{\ell}$ ;
- combined with the contribution akin to the second line of (14), the last statement extends to  $\ell' = \ell$ .

In conclusion, the dependence of vertices on external momenta is crucial to understand the integration of the flow equation. Formally this means that treating momentum-dependence of vertices requires the solution of a delay differential equation in  $\ell$ , where the delay is determined by the value of the external momenta. Practically, the resulting procedure is simple:

$$\Lambda_\ell = \frac{\Lambda}{\ell}$$

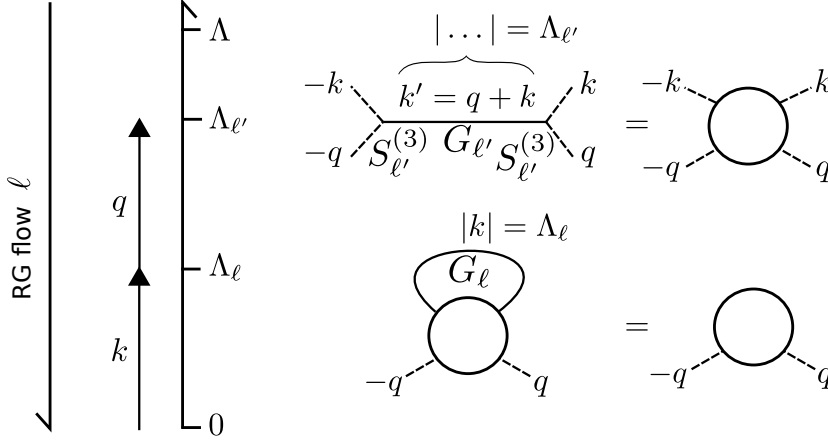


**Figure 1. Flow of momentum dependent vertex caused by decimation step.** An effective four-point vertex of reducible tree shape (top) is produced within decimation step  $\ell'$ . The shell  $\ell'$  in is determined by the momentum  $|k'| = |q + k| = \Lambda_{\ell'}$  on the propagator line  $G_{\ell'}$ . The propagator  $G_{\ell'}$  and the three-point vertices  $S_{\ell'}^{(3)}$  take the values of the corresponding RG step  $\ell'$ . Later in the flow, at  $\ell > \ell'$ , two legs of the four-point vertex are contracted to form a contribution to the two-point vertex  $S_\ell^{(2)}$  (self-energy). At fixed and given external momentum  $q$ , the decimation of shell  $\ell$  thus involves two four-point vertices  $S_{\ell'}$  and one propagator  $G_{\ell'}$  that take their values they had in the earlier shell  $\ell' < \ell$ .

- contributions from tree diagrams to the coarse-grained action can be integrated trivially; they have a non-vanishing value whenever the momenta of all propagators that connect the vertices of the tree are not below the current cutoff  $\Lambda_\ell$ ;
- only one-loop diagrams where a propagator connects to a single vertex contribute non-trivially to the flow; in such diagrams we need to replace the vertex by all reducible subgraphs, determined by the previous point; consequently, at non-zero external momenta there is only precisely one single-scale propagator, a propagator whose momentum is constrained to the shell of the current decimation step;
- the structure and combinatorial factors of the diagrams are identical to the usual one-loop fluctuation expansion; the appearance of precisely one single-scale propagator in the loop is structurally the same as in the Wetterich equation.

The coupling of different momentum shells arises only if one considers the dependence of vertices on external, non-zero momenta. As long as the flow of vertices is computed at vanishing external momenta, all propagator lines in a one-loop diagram necessarily lie on the same shell. This special case is treated in most text books and in the original review by Wilson [12]; it corresponds to diagrams appearing in the second line of (14).

The combination of vertices that belong to different momentum shells, at first sight, seems to be in contradiction to the required locality property of a flow equation, which is of general form  $\ell \frac{dK_\ell}{d\ell} = \frac{\partial T}{\partial \ell}(K_\ell, \ell)|_{\ell=1}$ , where  $K_\ell$  is a coupling and  $T$  a general coarse-graining operator [22]: the right hand side should only depend on the couplings  $K_\ell$  at the current scale  $\ell$ , not on the couplings of shells in the RG past  $\ell' < \ell$ ;

this property ensures that the semi-group composition law holds. This contradiction, however, is only apparent because the value of a reducible diagram does not change except for in the one particular shell  $\ell'$  which is determined by the momentum  $k$  of the connecting propagator,  $|k| = \Lambda_{\ell'}$ ; so the diagram has the same value at all later coarse-graining steps  $\ell > \ell'$ . If we kept track of the tree diagrams separately, they would “automatically” take the right value if combined into a loop diagram. This would mean, however, that we follow the flow of the action as a functional of  $\varphi(k)$  for all values of  $k$ . The direct insertion of tree diagrams can thus be considered a short cut to alleviate the book keeping.

### 2.6. Decimating an infinitesimal momentum shell

A decimation step of the form (17), where all tree-diagrams have been inserted, requires the computation of a one-loop integral. We here derive its concrete form. A one-loop integral across the momentum shell (9) is of the form

$$\begin{aligned} I_\delta &:= \int_{\Lambda_{\ell(1+\delta)} < |k| < \Lambda_\ell} f(k) \\ &= \frac{1}{(2\pi)^d} \int_{\Lambda_{\ell(1+\delta)}}^{\Lambda_\ell} dk k^{d-1} \int d\Omega f(\Omega \cdot k), \end{aligned} \quad (18)$$

where  $d\Omega$  is the angular integral. Now taking the limit  $\delta \rightarrow 0$  (12) we may expand the integral (18) in  $\delta$  to obtain

$$\begin{aligned} &\lim_{\delta \rightarrow 0} \frac{I_\delta}{\delta} \\ &= \lim_{\delta \rightarrow 0} \frac{1}{\delta} \left( \delta \ell \underbrace{\frac{d\Lambda_\ell}{d\ell}}_{-\frac{\Lambda}{2}} \frac{d}{d\Lambda_\alpha} \frac{1}{(2\pi)^d} \int_{\Lambda_\alpha}^{\Lambda_\ell} dk k^{d-1} \int d\Omega f(\Omega \cdot k) \Big|_{\Lambda_\alpha = \Lambda_\ell} + \mathcal{O}(\delta^2) \right) \\ &= \frac{\Lambda_\ell^d}{(2\pi)^d} \int d\Omega f(\Omega \cdot \Lambda_\ell). \end{aligned} \quad (19)$$

In the following we write for short

$$\int d\Omega f(\Omega \cdot \Lambda_\ell) \equiv \int_{|k|=\Lambda_\ell} f(k).$$

### 2.7. Rescaling of momenta and wavefunction renormalization

To find fixed points of the RG equations the length scale and hence the momentum scale are rescaled so that the ranges of momenta are the same before and after a coarse-graining step; otherwise there cannot possibly be any fixed points. It is common to define the new momenta  $k_\ell$  as (7). As a consequence these now span again the same space as did the  $k$  prior to any decimation

$$0 < |k_\ell| < \Lambda.$$

To express the coarse-grained action in the corresponding new field variables, one defines

$$\varphi_\ell(k_\ell) := \ell^{-1 - \frac{d-\eta}{2}} \varphi_<(q), \quad (20)$$

where the relation between  $k_\ell$  and  $q$  is fixed by (7) and we introduced the wavefunction renormalization factor  $\ell^{-1-\frac{d-\eta}{2}}$  and the anomalous dimension  $\eta$  as usual to keep the  $k^2$ -dependent coefficient  $r^{(2)}$  in (3) invariant under rescaling [12]: the factor  $\ell^{-1-\frac{d}{2}}$  is chosen such that the Gaussian theory alone would maintain scale-invariance, as shown in the following:

Our aim is to bring the coarse-grained action into the same form as the original Gaussian action at the expense of modified parameters. For the Gaussian part of the action (see also Section 5.1 for details), expressing  $\varphi_<$  by the rescaled field  $\varphi_\ell$  (20) yields, with the substitution  $\int_q \equiv \ell^{-d} \int_{k_\ell}$ ,

$$\begin{aligned} S_\ell[\varphi_<] &= \ln \mathcal{Z}_> - \frac{1}{2} \int_{0 \leq |q| < \Lambda_\ell} \varphi_<(-q) (r^{(0)} + r^{(2)} q^2) \varphi_<(q) \\ &= \ln \mathcal{Z}_> - \frac{1}{2} \ell^{2+d-\eta} \ell^{-d} \int_{0 \leq |k_\ell| < \Lambda} \varphi_\ell(-k_\ell) (r^{(0)} + r^{(2)} \ell^{-2} k_\ell^2) \varphi_\ell(k_\ell). \end{aligned} \quad (21)$$

So the coefficient of the  $k_\ell^2$ -dependent term must be chosen as

$$r_\ell^{(2)} := r^{(2)} \ell^{-\eta}, \quad (22)$$

for the action to maintain the same form. Analogously the parameter  $r_\ell^{(0)}$ , the coefficient of  $\varphi^2$ , is read off from (21) as

$$r_\ell^{(0)} := r^{(0)} \ell^{2-\eta}. \quad (23)$$

Performed infinitesimally, the rescaling step thus contributes

$$\ell \frac{dr_\ell^{(0)}}{d\ell} = (2 - \eta) r_\ell^{(0)} + \dots, \quad (24)$$

$$\ell \frac{dr_\ell^{(2)}}{d\ell} = -\eta r_\ell^{(2)} + \dots, \quad (25)$$

Here the ellipses are the terms from the decimation step.

Correspondingly, the interaction terms  $S_\ell^{(n>2)}$  transform under the rescaling

$$\begin{aligned} &\int_{q_1} \dots \int_{q_{n-1}} S^{(n)}(\{q\}) \varphi_<^n(q) \\ &= \ell^n \left(1 + \frac{d-\eta}{2}\right) \int_{k_{\ell,1}} \dots \int_{k_{\ell,n-1}} \ell^{-d} \dots \int_{k_{\ell,n-1}} \ell^{-d} S^{(n)}(\ell^{-1}\{k_\ell\}) \varphi_\ell^n(k_\ell), \end{aligned}$$

so that the coarse-grained coefficients are defined as

$$\begin{aligned} S_\ell^{(n)}(\{k_\ell\}) &:= \ell^n \left(1 + \frac{d-\eta}{2}\right) - (n-1)d S^{(n)}(\ell^{-1}\{k_\ell\}) \\ &= \ell^n \left(1 - \frac{d+\eta}{2}\right) + d S^{(n)}(\ell^{-1}\{k_\ell\}). \end{aligned} \quad (26)$$

We would like to express the rescaling now for an infinitesimal change of scale, as we did for (24). We obtain from (26)

$$\begin{aligned} \ell \frac{dS_\ell^{(n)}(\{k_\ell\})}{d\ell} &= \left(n \left(1 - \frac{d+\eta}{2}\right) + d\right) S_\ell^{(n)}(\{k_\ell\}) \\ &\quad - k_\ell \frac{dS_\ell^{(n)}(\{k_\ell\})}{dk_\ell}, \end{aligned} \quad (27)$$

where we used the chain rule to obtain the second term.

Since we perform the coarse-graining and the rescaling for an infinitesimal step  $\delta \rightarrow 0$ , the right hand sides of (13) and (27) simply add up to produce the final flow equation; cross terms are of order  $\mathcal{O}(\delta^2)$  and hence drop out in the infinitesimal formulation.

### 2.8. Treating momentum dependence in the $\varphi^4$ -theory

At the end of Section 2.5 the dependence on external momenta was identified as the reason why different decimation steps need to be combined to form the one-loop diagrams that cause the flow in a given shell. In particular, it was shown that the momentum-dependence leads to a functional delay-differential equation in  $\ell$ , where the delay is a function of the external momentum. This section explicitly treats this momentum dependence on the example of the  $\varphi^4$  theory (3) to obtain an improved solution for the anomalous dimension beyond its leading order approximation  $\eta = 0$ .

For conceptual clarity, consider the continuous flow equation as a result of a sequence of decimation and rescaling steps with an infinitesimal thickness of  $\delta$  for each shell, where in the  $i$ -th step the flow parameter assumes the value

$$\ell_i = 1 + i \cdot \delta.$$

We write for short for a momentum  $k \in i$  to denote that it is within the  $i$ -th shell, namely

$$\Lambda_{\ell_{i+1}} < |k| < \Lambda_{\ell_i} \quad \leftrightarrow \quad k \in i.$$

*Decimation* We here investigate the flow for momentum-dependent vertices on the example of the four point vertex. This is illustrated in Figure 2, where the flow parameter  $\ell = 1, \dots, \infty$  runs from top to bottom. Each decimation step performs the marginalization of the modes  $\varphi(k)$  that belong to the shell  $k \in i$ .

Above, we have distinguished two classes of graphs. The tree-shaped graphs are simple: They contain a single chain of propagators. The momentum  $k$  of the contracted pair of fields belongs to precisely one decimation step, the step for which  $k \in i$ . In Figure 2, the  $i$ -th step contributes a tree shaped diagram of two four point vertices; it thus yields a contribution to the six-point vertex, because there are six uncontracted fields  $\varphi_<$  left. The value of the propagator is the one that belongs to the corresponding shell, because it results from the marginalization of the corresponding modes. For spherically symmetric propagators, its value is  $G_{\ell_i}(\Lambda_{\ell_i})$ . The entire contribution to the coarse-grained action is therefore

$$S^{(6)}(q_1, \dots, q_6) = 4 \cdot 4 \cdot \frac{1}{2!} \left( \frac{S_{\ell_i}^{(4)}}{4!} \right)^2 G_{\ell_i}(q_1 + q_2 + q_3). \quad (28)$$

Correspondingly, it holds that

$$q_1 + q_2 + q_3 \in i. \quad (29)$$

The combinatorial factor  $4 \cdot 4$  caters for the number of possible legs to choose from to be contracted; the factor  $1/2!$  stems from the appearance of two vertices.

Now consider a contribution to the four-point vertex at non-vanishing external momenta  $q_1 + q_2 \neq 0$ , as shown in Figure 2, bottom. The contribution is composed of the six-point vertex (28) with two legs contracted. The decimation step must necessarily be  $j \geq i$ , for otherwise the six-point vertex would not exist, so

$$q_3 \in j. \quad (30)$$

$$\Lambda_\ell = \frac{\Lambda}{\ell} \quad \ell_i = 1 + i\delta$$

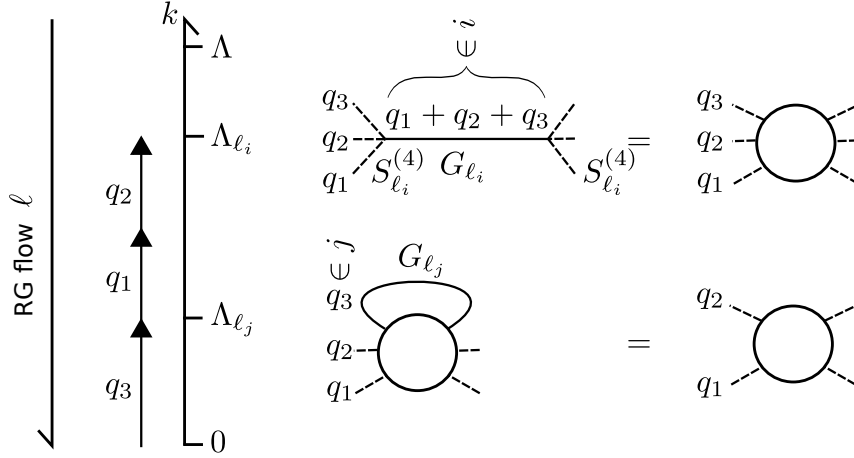


**Figure 2. Flow of momentum dependent vertex from the decimation step.** An effective six-point vertex of reducible tree shape (top) is produced within decimation step  $i$ . The shell  $i$  in which the six-point vertex is produced is determined by the momentum  $q_1 + q_2 + q_3 \in i$  on the propagator line  $G_{\ell_i}$ . The propagator  $G_{\ell_i}$  and the four-point vertices  $S_{\ell_i}^{(4)}$  take the values of the corresponding RG step  $i$ . Later in the flow, at  $j > i$ , two legs of the six-point vertex are contracted to form a contribution to the four-point vertex  $S_{\ell_j}^{(4)}$ . For given external momenta  $q_1, q_2$ , the integration over the loop momentum  $q_3$  thus involves six point vertices produced in different shells  $i$ .

The contribution to the flow of the four point vertex therefore reads

$$\ell \frac{1}{4!} \frac{dS_\ell^{(4)}}{d\ell} = \underbrace{4 \cdot 4 \cdot 3 \cdot 3}_{=36} \cdot \frac{1}{2} \cdot \frac{1}{2!} \frac{1}{(2\pi)^d} \int_{|q_3|=\Lambda_j} \left( \frac{S_{\ell_i}^{(4)}}{4!} \right)^2 G_{\ell_i}(q_1 + q_2 + q_3) G_{\ell_j}(q_3), \quad (31)$$

where the combinatorial factor  $3 \cdot 3 \cdot \frac{1}{2}$  represents the combinations of selecting a pair of the legs of the six point vertex from the two sets of three legs each. The factor  $1/2$  has the same reason as in an  $n$  choose 2 factor: the order by which we pick the pair does not matter, so we need to correct for this factor, since we otherwise double-count contractions. The combinatorial factor in total is  $4 \cdot 4 \cdot 3 \cdot 3 \cdot \frac{1}{2} = 72$ , identical to that of the usual one loop diagram.

*Rescaling* To obtain the scaling form of the flow equation, we need to perform the rescaling of fields and momenta, as described in [Section 2.7](#).

The six point vertex is generated in the step  $i < j$ . In the rescaled units, the momenta in step  $i$  and step  $j$  obey, with [\(7\)](#), the relation

$$k = \ell_j q.$$

The six point vertex, expressed in terms of the quantities at the scale  $\ell_j$ , with [\(26\)](#), is

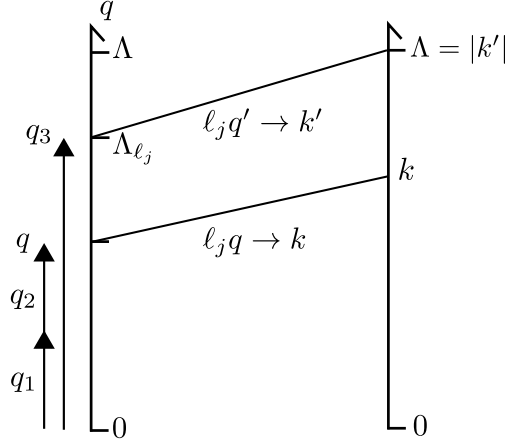


**Figure 3. Rescaling of momenta.** Momenta  $q$  before rescaling. Here  $q_1$  and  $q_2$  are external momenta and  $q_3 = q'$  is the loop momentum in (31). Momenta  $k = \ell_j q$  after rescaling. The rescaled loop momentum  $k' = \ell_j q'$  is located at the cutoff of the decimation step,  $|k'| = \Lambda$ .

$$S_{\ell_j}^{(n)}(\{k\}) = \ell_j^{n(1-\frac{d+n}{2})+d} S^{(n)}(\ell_j^{-1}\{k\}).$$

Conversely, we need to express  $S^{(n)}$  in terms of the rescaled coefficient at scale  $i$ , for which the same relation holds, but with  $i \leftrightarrow j$ , so that we get in total

$$S_{\ell_j}^{(n)}(\{k\}) = \left(\frac{\ell_j}{\ell_i}\right)^{n(1-\frac{d+n}{2})+d} S_{\ell_i}^{(n)}\left(\frac{\ell_i}{\ell_j}\{k\}\right).$$

So only the ratio  $\ell_i/\ell_j$  of the coarse-graining scale parameter appears. This ratio, in turn, is related to the momenta by (29) and (30) with  $q := q_1 + q_2$  and  $q' := q_3$  as  $|q + q'| = \frac{\Lambda}{\ell_i}$  and  $|q'| = \frac{\Lambda}{\ell_j}$  we have

$$\frac{\ell_j}{\ell_i} = \frac{|q' + q|}{|q'|}. \quad (32)$$

Here the momenta  $q$  and  $q'$  are measured at the absolute scale, as shown in Figure 2 — they are the arguments of  $\varphi_{<}(q)$ . But we want to know how the four point vertex depends on the momenta of the fields  $\varphi_{\ell_j}(k)$ . We thus need to express the momentum  $q$  that appears in the latter factor by the  $k$  at scale  $\ell_j$ , as illustrated in Figure 3. The coarse-graining scale  $\ell_j$  satisfies  $\ell_j|q'| \equiv \ell_j|q_3| = \Lambda$ . At this scale, the momenta  $q$  take the value  $\ell_j q =: k$ , so

$$q = \frac{1}{\ell_j} k = \frac{|q'|}{\Lambda} k,$$

$$q' = \frac{1}{\ell_j} k' = \frac{|q'|}{\Lambda} k'.$$

We thus have

$$\left(\frac{\ell_j}{\ell_i}\right)^2 = \frac{(q' + q)^2}{q'^2} = \frac{(k' + k)^2}{\Lambda^2}. \quad (33)$$

Expressed in rescaled variables, the correction (31) to the four-point vertex hence takes the form

$$\begin{aligned}
 & 3 \cdot 3 \cdot \frac{1}{2} \cdot \frac{1}{(2\pi)^d} \int_{|k'|=\Lambda} \theta(\ell_i - \ell_j +) \left( \frac{\ell_j}{\ell_i} \right)^{6 \left(1 - \frac{d+\eta}{2}\right) + d} \frac{S_{\ell_i}^{(6)} \left( \frac{\ell_i}{\ell_j} \{k\} \right)}{6!} G_{\ell_j}(k') \quad (34) \\
 &= \underbrace{36}_{4 \cdot 4 \cdot 3 \cdot 3 \cdot \frac{1}{2} \cdot \frac{1}{2!}} \cdot \frac{1}{(2\pi)^d} \int_{|k'|=\Lambda} \theta(\ell_i - \ell_j +) \left( \frac{\ell_j}{\ell_i} \right)^{6 \left(1 - \frac{d+\eta}{2}\right) + d} \left( \frac{S_{\ell_i}^{(4)} \left( \frac{\ell_i}{\ell_j} \{k\} \right)}{4!} \right)^2 G_{\ell_i}(\Lambda) G_{\ell_j}(\Lambda) \\
 &\simeq 36 \cdot \frac{1}{(2\pi)^d} \left( \frac{S_*^{(4)}}{4!} \right)^2 \int_{|k'|=\Lambda} 1 + \theta(k' \cdot k +) \left( 6 - 2d - 3\eta \right) \times \quad (35) \\
 &\quad \times \left( \frac{(k' \cdot k)}{\Lambda^2} + \frac{k^2}{2\Lambda^2} + \frac{(k' \cdot k)^2}{\Lambda^4} \left( 2 - d - \frac{3}{2}\eta \right) \right) G_{\ell_i}(\Lambda) G_{\ell_j}(\Lambda).
 \end{aligned}$$

From the second to the third line we expanded the term  $\left( \frac{\ell_j}{\ell_i} \right)^{6 \left(1 - \frac{d+\eta}{2}\right) + d}$  up to second order in  $k'$  by using (33) (see Section 5.2 for details). The notation  $\theta(x+)$  is to be read as  $\lim_{\epsilon \searrow 0} \theta(x + \epsilon)$ . The Heaviside functions ensure that the effective six-point vertex has already been produced at the decimation step  $i$ , namely that  $\ell_i \geq \ell_j$ . In the last line, we rewrite this condition, amounting to  $|k + k'| > |k'|$  as  $k$  and  $k'$  having a parallel component,  $\theta(k' \cdot k +)$ .

The four point vertices  $S_{\ell_i}^{(4)}$  and the propagator  $G_{\ell_i}$  that appear here are those expressed in terms of the rescaled variables at scale  $\ell_i$ , because they take the values they had in the  $i$ -th decimation step. The momentum of each propagator in rescaled units is always equal to the original cutoff. In the last step we assumed that the flow will be close to the fixed point. As a result, we may replace the vertices and the propagators by their values at the fixed point, denoted by a star.

In addition, in the last step we neglected the effect of the momentum dependence of  $S^{(4)}$  on its own corrections. We will a posteriori see that the neglected terms are at most of order  $(u_*^{(0)})^3$ , where  $u_*^{(0)}$  is the momentum-independent part of the interaction. This approximation is good as long as the interaction is small. In principle, the momentum-dependence of  $S^{(4)}$  can be taken into account at the expense of additional computations.

If we assumed  $d = 4$  and  $\eta = 0$ , the last line in (35) would simplify to

$$36 \cdot \frac{1}{(2\pi)^4} \int_{|k'|=\Lambda} \frac{\theta(k' \cdot k +) \Lambda^2}{(k' + k)^2} \left( \frac{S_*^{(4)}}{4!} \right)^2 G_*(\Lambda) G_*(\Lambda). \quad (36)$$

This approximation is justified if one wants to compute the correction only in  $d = 4 - \epsilon$  dimensions, in which case  $\eta \propto \epsilon^2$ , as will be seen in the following. In the following we do not make this approximation, but rather keep the full dependence on  $d$  and  $\eta$  in (35).

The main insight of this section is the appearance of the first factor in the last line of (35) that, by (29), arises from the rescaling term in combination with the momentum-dependence of the shell index  $\ell_i(q_1 + q_2 + q_3)$ . The latter implies a dependence on the external momenta  $q_1 + q_2$  of the effective four-point vertex. It is



a direct consequence of the insertion of the tree diagram produced in the decimation step  $\ell_i$  previous to the current one,  $\ell_j$ ; showing that we solve a delayed functional differential equation here. This momentum-dependence has been neglected in the approximation made in [13], as discussed below.

### 2.9. Flow of the momentum dependent interaction vertex

We are interested in the long-distance behavior for which we want to get a flow equation. This requires the momentum dependence of (34) for small  $k$ .

We here study the case that the dimensionality of the system is not close to the upper critical dimension, thus  $d \neq 4 - \epsilon$ . One then cannot make the approximation in (36), but rather needs to use the full expression (35). The computation is, however, not more complicated than the approximation, because for up to order  $\mathcal{O}(k^2)$  the same integrals appear. These are (details are given in the Appendix Section 5.4, (83), (84))

$$\begin{aligned} \int_{|k'|=\Lambda} \theta(k' \cdot k_+) (k' \cdot k) &= S_{d-1} \Lambda \|k\| \frac{1}{d-1}, \\ \int_{|k'|=\Lambda} \theta(k' \cdot k_+) k^2 &= \frac{S_d}{2} k^2, \\ \int_{|k'|=\Lambda} \theta(k' \cdot k_+) (k' \cdot k)^2 &= \frac{S_d}{2d} \Lambda^2 k^2. \end{aligned}$$

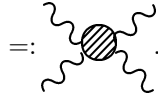
We thus obtain from the decimation step and (35)

$$\begin{aligned} \ell \frac{d}{d\ell} \frac{1}{4!} S_\ell^{(4)}(k_1, k_2, k_3, k_4) & \quad (37) \\ = 36 \frac{\Lambda^d}{(2\pi)^d} (u_\ell^{(0)})^2 G_\ell^2(\Lambda) & \left[ S_d + (6 - 2d - 3\eta) \times \right. \\ \times \left( \frac{S_{d-1}}{d-1} \frac{\|k_1 + k_2\|}{\Lambda} + \frac{S_d}{4d} (4 - d - 3\eta) \frac{(k_1 + k_2)^2}{\Lambda^2} \right) & \left. \right]. \end{aligned}$$

Had we taken the momentum-dependence of  $S^{(4)}$  into account (see comment after (35)), we would have gotten additional terms here. We will a posteriori see that the neglected terms are of order  $\mathcal{O}((u_*^{(0)})^3)$  and discuss their importance close to  $d = 3$  after eq. (52).

So the renormalized action requires a momentum-dependent  $S^{(4)}$ -interaction of the form

$$-\frac{1}{4!} S_\ell^{(4)}(k_1, k_2, k_3, k_4) = u_\ell^{(0)} + u_\ell^{(1)} \|k_1 + k_2\| + u_\ell^{(2)} (k_1 + k_2)^2 \quad (38)$$



Defining the rescaled parameters with subscript  $\ell$ , according to (26) with  $n = 4$  yields

$$\begin{aligned} -\frac{1}{4!} S_\ell^{(4)}(k_{\ell 1}, k_{\ell 2}) & =: u_\ell^{(0)} + u_\ell^{(1)} \|k_{\ell 1} + k_{\ell 2}\| + u_\ell^{(2)} (k_{\ell 1} + k_{\ell 2})^2 & (39) \\ & \stackrel{(26)}{=} \ell^{4-d-2\eta} (u^{(0)} + u^{(1)} \ell^{-1} \|k_{\ell 1} + k_{\ell 2}\| + u^{(2)} \ell^{-2} (k_{\ell 1} + k_{\ell 2})^2). \end{aligned}$$

In differential form the contribution from rescaling is thus

$$\ell \frac{d}{d\ell} u_\ell^{(0)} = (4 - d - 2\eta) u_\ell^{(0)} + \dots, \quad (40)$$

$$\ell \frac{d}{d\ell} u_\ell^{(1)} = (3 - d - 2\eta) u_\ell^{(1)} + \dots, \quad (41)$$

$$\ell \frac{d}{d\ell} u_\ell^{(2)} = (2 - d - 2\eta) u_\ell^{(2)} + \dots, \quad (42)$$

where the momentum-dependent term  $k_\ell \frac{dS_\ell^{(n)}(k_\ell)}{dk_\ell}$  in (27) is taken care of by explicitly rescaling the momenta appearing in (39).

The complete flow equations of the parameters  $u_\ell^{(0)}$ ,  $u_\ell^{(1)}$ , and  $u_\ell^{(2)}$  then follow by including the decimation step (37) as

$$\begin{aligned} \ell \frac{du_\ell^{(0)}}{d\ell} &= (4 - d - 2\eta) u_\ell^{(0)} \\ &\quad - 36 S_d \frac{\Lambda^d}{(2\pi)^d} \frac{(u_\ell^{(0)})^2}{(r_\ell^{(0)} + r_\ell^{(2)} \Lambda^2)^2}, \end{aligned} \quad (43)$$

$$\begin{aligned} \ell \frac{du_\ell^{(1)}}{d\ell} &= (3 - d - 2\eta) u_\ell^{(1)} \\ &\quad - 36 (6 - 2d - 3\eta) \frac{S_{d-1}}{d-1} \frac{\Lambda^d}{(2\pi)^d} \frac{(u_\ell^{(0)})^2}{(r_\ell^{(0)} + r_\ell^{(2)} \Lambda^2)^2} \frac{1}{\Lambda}, \end{aligned} \quad (44)$$

$$\begin{aligned} \ell \frac{du_\ell^{(2)}}{d\ell} &= (2 - d - 2\eta) u_\ell^{(2)} \\ &\quad - 36 (6 - 2d - 3\eta) (4 - d - 3\eta) \frac{S_d \Lambda^d}{4d (2\pi)^d} \frac{(u_\ell^{(0)})^2}{(r_\ell^{(0)} + r_\ell^{(2)} \Lambda^2)^2} \frac{1}{\Lambda^2}. \end{aligned} \quad (45)$$

The flow equation for  $u_\ell^{(2)}$  has the property that for  $d = 3$  the first factor in the second row is  $-3\eta$  and for  $d = 4$ , the second factor becomes  $-3\eta$ ; this means that the quadratic momentum dependence in both cases becomes small,  $u_\ell^{(2)}/(u_\ell^{(0)})^2 \propto \eta$ . In between these two limits, the corrections are larger. The flow equation for  $u_\ell^{(1)}$  has a first factor that is  $\propto -3\eta$  for  $d = 3$ . But at the same time, the rescaling term becomes  $-2\eta$ , so  $\eta$  drops out of the fixed point equation. The  $|k|$ -dependence of the interaction will thus dominate over the  $k^2$ -dependence in  $d = 3$  dimensions. This is an example that shows that the non-differentiable  $k$ -dependence may become important.

By the rescaling, we express propagators and vertices in the correction terms by the ones at the initial scale, as given by (27). This also replaces  $\Lambda_\ell \rightarrow \Lambda$ , because the rescaling after each decimation step restores the original range of momenta and thus keeps the position of the cutoff constant.

### 2.10. Flow of the momentum-dependent self-energy

Inserting the momentum-dependent term of the interaction  $S_\ell^{(4)}$  (38) into the self-energy corrections, this interaction vertex induces a dependence on  $k$ . We have two possibilities of inserting the interaction into the self-energy diagram

$$= \varphi_{<}(q) \varphi_{<}(-q) \frac{4 \cdot 3}{2} \frac{\Lambda^d}{(2\pi)^d} \int_{|k|=\Lambda} \frac{1}{4!} S_\ell^{(4)}(-q, q, k, -k) G_\ell(k),$$

which leads to the second and third line of the following equation

$$\ell \frac{d}{d\ell} \frac{1}{2} S_\ell^{(2)}(q, -q) := -2 \cdot 6 \cdot \quad (46)$$

$$= -2 \cdot 2 \cdot \frac{\Lambda_\ell^d}{(2\pi)^d} \cdot \int_{|k|=\Lambda_\ell} \frac{1}{4!} S_\ell^{(4)}(q, -q, k, -k) G_\ell(k)$$

$$- 2 \cdot 4 \cdot \frac{\Lambda_\ell^d}{(2\pi)^d} \cdot \int_{|k|=\Lambda_\ell} \frac{1}{4!} S_\ell^{(4)}(q, k, -k, -q) G_\ell(k).$$

The penultimate line corresponds to the 2 ways of choosing either the left pair or the right pair of amputated legs of the interaction vertex  $S^{(4)}$  to be the amputated lines of the self-energy diagram – in both cases we have  $q_1 = q$  and  $q_2 = -q$ , so that the momentum dependence of the four point vertex  $S^{(4)}(q, -q, k, -k)$ , according to eq. (38), drops out. In the latter row the four point vertex is inserted such that one external amputated leg connects to left side of  $S^{(4)}$  (2 possibilities) and one to the right side (another 2 possibilities), so we get a term

$$\frac{1}{4!} S_\ell^{(4)}(q, k, -k, -q) = u_\ell^{(0)} + u_\ell^{(1)} \sqrt{(q+k)^2} + u_\ell^{(2)} (q+k)^2, \quad (47)$$

which therefore is dependent on the momentum  $q$ . Dropping terms of order  $\mathcal{O}(q^3)$  and higher and sorting the result into terms  $\propto q^0$  and  $\propto q^2$  according to  $-S^{(2)}(q) = r_\ell^{(0)} + r_\ell^{(2)} q^2 + \mathcal{O}(q^3)$  we get the pair of flow equations (see Section 5.5 for details)

$$\ell \frac{d}{d\ell} r_\ell^{(0)} = (2 - \eta) r_\ell^{(0)} \quad (48)$$

$$+ 2 \cdot \frac{S_d \Lambda^d}{(2\pi)^d} \cdot \frac{6 u_\ell^{(0)} + 4 u_\ell^{(1)} \Lambda + 4 u_\ell^{(2)} \Lambda^2}{r_\ell^{(0)} + r_\ell^{(2)} \Lambda^2},$$

$$\ell \frac{d}{d\ell} r_\ell^{(2)} = -\eta r_\ell^{(2)} \quad (49)$$

$$+ 8 \cdot \frac{S_d \Lambda^d}{(2\pi)^d} \cdot \frac{\frac{u_\ell^{(1)}}{2\Lambda} \left(1 - \frac{1}{d}\right) + u_\ell^{(2)}}{r_\ell^{(0)} + r_\ell^{(2)} \Lambda^2},$$

where the first line in each flow equation comes from the rescaling given by (24) and (25). The momentum dependence of the propagator  $G_\ell(q) \equiv (-S^{(2)}(q))^{-1}$  here follows from the momentum dependence of  $S^{(2)}(q)$ ; so only a constant and a  $k^2$ -dependent term arises in the inverse propagator.

2.11. Fixed points and critical exponents for  $3 \leq d \leq 4$ 

We may now compute the Wilson-Fisher fixed point for arbitrary dimensions between 3 and 4. We determine  $\eta$  such that  $r_*^{(2)} \equiv 1$  is a fixed point of (49). Throughout we approximate the mass to be small compared to the cutoff,  $r_*^{(0)} \ll \Lambda^2$ . The details can be found in Section 5.6.

*Interaction* The fixed point for the momentum-independent four point coupling obeys

$$\Lambda^{d-4} u_*^{(0)} \simeq (2\pi)^d \frac{4-d-2\eta}{36 S_d}. \quad (50)$$

In the limits  $d \rightarrow 3$  and  $d \rightarrow 4$  we get

$$\Lambda^{d-4} u_*^{(0)} \simeq \begin{cases} \pi^2 \frac{1-2\eta}{18} \simeq \frac{\pi^2}{18} & d = 3 \\ \pi^2 \frac{2}{9} (\epsilon - 2\eta) & d = 4 - \epsilon \end{cases}. \quad (51)$$

As explained by Wilson [12, section V], all fixed point values can be related back to the value of the interaction  $u_*^{(0)}$ , the single marginal coupling of the Gell-Mann-Low theory. The first-order momentum dependence is quadratic in  $u_*^{(0)}$

$$\Lambda^{5-d} \frac{u_*^{(1)}}{(u_*^{(0)})^2} \simeq \frac{36}{(2\pi)^d} \frac{2(3-d) - 3\eta}{3-d-2\eta} \frac{S_{d-1}}{d-1}. \quad (52)$$

As long as  $u_0$  is small, this justifies the approximation made in the last line of (35), the neglect of the momentum-dependence of the four-point vertex. Close to  $d = 4$  dimensions this approximation is very good, as expected. As  $d \rightarrow 3$  dimensions are approached, the error increases, because with (51)  $\Lambda^{d-4} u_*^{(0)} \simeq \pi^2/18 \simeq 1/2$ .

In the limits  $d \rightarrow 3$  and  $d \rightarrow 4$  we get

$$\Lambda^{d-3} u_*^{(1)} \simeq \begin{cases} \frac{\pi^2}{48} (1-2\eta)^2 \simeq \frac{\pi^2}{48} & d = 3 \\ \frac{4}{9} \frac{2(1+\epsilon)-3\eta}{1+\epsilon-2\eta} (\epsilon-2\eta)^2 \frac{\pi}{(3-\epsilon)} \simeq \frac{8\pi}{27} \epsilon^2 + \mathcal{O}(\epsilon^3) & d = 4 - \epsilon \end{cases}. \quad (53)$$

The quadratic momentum dependence of the interaction is

$$\Lambda^{6-d} \frac{u_*^{(2)}}{(u_*^{(0)})^2} \simeq 36 \frac{S_d}{(2\pi)^d} \frac{2(3-d) - 3\eta}{2-d-2\eta} \frac{4-d-3\eta}{4d}. \quad (54)$$

As expected from the  $\epsilon$ -expansion, the fixed-point value depends quadratically on  $u_*^{(0)}$ . For  $d \rightarrow 3$  and  $d \rightarrow 4$  we get

$$\Lambda^{d-2} u_*^{(2)} \simeq \begin{cases} \frac{\pi^2}{72} \frac{\eta}{1+2\eta} (1-3\eta)(1-2\eta+4\eta^2) \simeq \frac{(2\pi)^3}{72} \eta + \mathcal{O}(\eta^2) & d = 3 \\ \frac{2\pi^2}{9} \frac{2(1-\epsilon)+3\eta}{2-\epsilon+2\eta} \frac{(\epsilon-3\eta)(\epsilon-2\eta)^2}{4(4-\epsilon)} \simeq \frac{\pi^2}{72} \epsilon^3 + \mathcal{O}(\epsilon^4) & d = 4 - \epsilon \end{cases}. \quad (55)$$

*Mass term* To check if the approximation  $r_*^{(0)} \ll \Lambda^2$  is justified, one observes that the fixed point value for  $r_*^{(0)}$ , in this approximation, is determined as

$$\begin{aligned} \Lambda^{-2} r_*^{(0)} &\simeq - \frac{6 S_d}{(2\pi)^d} \cdot \Lambda^{d-4} u_*^{(0)} \\ &- \frac{144 S_d}{(2\pi)^{2d}} \frac{2(3-d) - 3\eta}{3-d-2\eta} \left( \frac{S_{d-1}}{d-1} + \frac{4-d-3\eta}{4d} S_d \right) (\Lambda^{d-4} u_*^{(0)})^2, \end{aligned} \quad (56)$$

which shows the approximate linear relationship between  $r_*^{(0)}$  and  $u_*^{(0)}$  and explains why the mass term stays small as long as  $u_*^{(0)}$  is small. In this case, it is justified to approximate  $\Lambda^2 + r_*^{(0)} \rightarrow r_*^{(0)}$ . The ratio between mass and coupling term is

$$\begin{aligned} \Lambda^{2-d} \frac{r_*^{(0)}}{u_*^{(0)}} &\simeq - \frac{6 S_d}{(2\pi)^d} \\ &- \frac{4}{(2\pi)^d} \frac{(2(3-d) - 3\eta)(4-d-2\eta)}{3-d-2\eta} \left( \frac{S_{d-1}}{d-1} + \frac{4-d-3\eta}{4d} S_d \right). \end{aligned} \quad (57)$$

The correction to the linear relation in the second line is  $\propto \eta$  for  $d = 4$ , but becomes notable in for  $d < 3$ , as shown in [Figure 4c](#). Inserting the expression for  $u_*^{(0)}$  from [\(50\)](#) yields  $r_*^{(0)}$  as a function of  $d$ , shown in [Figure 4a](#).

*Critical exponent  $\eta$*  Demanding stationarity of [\(49\)](#) and  $r_\ell^{(2)} \stackrel{!}{=} 1$  we get

$$\eta = 8 \cdot \frac{S_d}{(2\pi)^d} \cdot \left( \frac{1}{2} \Lambda^{d-3} u_*^{(1)} \left( 1 - \frac{1}{d} \right) + \Lambda^{d-2} u_*^{(2)} \right). \quad (58)$$

Expressed in terms of  $u_*^{(0)}$

$$\begin{aligned} \Lambda^{8-2d} \frac{\eta}{(u_*^{(0)})^2} &\simeq 8 \frac{S_d}{(2\pi)^{2d}} \cdot \left( \frac{1}{2} \left( 1 - \frac{1}{d} \right) 36 \frac{2(3-d) - 3\eta}{3-d-2\eta} \frac{S_{d-1}}{d-1} \right. \\ &\quad \left. + 36 \frac{2(3-d) - 3\eta}{2-d-2\eta} \frac{4-d-3\eta}{4d} S_d \right). \end{aligned} \quad (59)$$

This expression has a factor  $\Lambda^{2d-8} (u_*^{(0)})^2$  appearing in both terms. So, as expected, expressing  $u_*^{(0)}$  by [\(50\)](#) one obtains a universal result that does not depend on  $\Lambda$ , the microscopic details of the system, reorganized as a cubic equation of which we need to determine the roots

$$\begin{aligned} 0 &\simeq \frac{8}{36} \frac{1}{S_d} \frac{2(3-d) - 3\eta}{d} \left( \frac{S_{d-1}}{2} (2-d-2\eta) \right. \\ &\quad \left. + \frac{S_d}{4} (3-d-2\eta) (4-d-3\eta) \right) (4-d-2\eta)^2 - \eta (3-d-2\eta) (2-d-2\eta). \end{aligned} \quad (60)$$

For  $3 < d \leq 4$ , we solve the cubic equation for  $\eta$  numerically. The result is shown in [Figure 4b](#).

Dropping from this cubic equation in  $\eta$  all terms that are  $\mathcal{O}(\eta^2)$ , for  $d = 4$  we get a linear equation in  $\eta$ , relating it to  $(u_*^{(0)})^2$  as

$$\begin{aligned}\eta &\simeq \frac{1}{16\pi^8} \frac{9S_4S_3}{2 + \frac{1}{64\pi^8} (27S_4^2 - 90S_4S_3) (u_*^{(0)})^2} (u_*^{(0)})^2 \\ &\simeq \frac{1}{16\pi^8} \frac{9S_4S_3}{2} (u_*^{(0)})^2 + \mathcal{O}((u_*^{(0)})^4) \\ &= \frac{9}{4\pi^5} (u_*^{(0)})^2 + \mathcal{O}((u_*^{(0)})^4) \\ &\simeq 0.0074 (u_*^{(0)})^2 + \mathcal{O}((u_*^{(0)})^4).\end{aligned}\tag{61}$$

With  $u_*^{(0)} \simeq \pi^2 \frac{2}{9} \epsilon + \mathcal{O}(\epsilon^2)$  (cf. (51)) one sees that this result is consistent with the limiting expressions for  $d = 4 - \epsilon$  for  $u_*^{(1)} \simeq \frac{8\pi}{27} \epsilon^2 + \mathcal{O}(\epsilon^3)$  (cf. (53)) and  $u_*^{(2)} = \frac{\pi^2}{72} \epsilon^3 + \mathcal{O}(\epsilon^4)$  inserted into (58) to find

$$\eta \simeq \frac{1}{9\pi} \epsilon^2 + \mathcal{O}(\epsilon^3).\tag{62}$$

The latter consideration shows that the  $\|k\|$ -dependence of the interaction  $u$  ( $\propto u_*^{(1)}$ ) causes the anomalous dimension close to four dimensions and the  $k^2$ -dependence of the interaction ( $\propto u_*^{(2)}$ ) only plays a role at higher orders  $\mathcal{O}(\epsilon^3)$ .

The value for  $\eta$  (62) is by a factor  $6/\pi \simeq 1.9$  larger than the two-loop result from the  $\epsilon$  expansion to second order [3, p. 626]

$$\begin{aligned}\eta &\simeq \frac{1}{54} \epsilon^2 \\ &\simeq \frac{9}{24\pi^4} (u_*^{(0)})^2 \\ &\simeq 0.0038 (u_*^{(0)})^2.\end{aligned}\tag{63}$$

For  $d = 3$  we obtain a quadratic equation from (60)

$$\begin{aligned}0 &\simeq \eta^2 + \frac{17S_3 + 2S_2}{43S_3 + 4S_2} \eta - \frac{S_2}{43S_3 + 4S_2} \\ 0 &\simeq \eta^2 + \frac{72}{180} \eta - \frac{1}{90},\end{aligned}$$

so

$$\begin{aligned}\eta_{\pm}^{(d=3)} &= -\frac{36}{180} \pm \sqrt{\left(\frac{36}{180}\right)^2 + \frac{1}{90}} \\ &= \begin{cases} 0.0261 & + \\ -0.426 & - \end{cases}.\end{aligned}\tag{64}$$

The positive solution is the physically relevant one.

*Critical exponent  $\nu$*  The critical exponent  $\nu$  is determined by linearizing the flow about the fixed point and by determining the eigenvalue  $\lambda_r$  in the direction of the parameter  $r$ . The critical exponent then takes the value

$$\begin{aligned}\nu &= \lambda_r^{-1} \\ &= \frac{1}{2 - \eta - \frac{1}{18} (4 - d - 2\eta)(2(3 - d) - 3\eta) \left( \frac{6}{2(3-d)-3\eta} + \frac{4}{d-1} \frac{4-d-2\eta}{3-d-2\eta} \frac{S_{d-1}}{S_d} + \frac{1}{d} \frac{(4-d-3\eta)(4-d-2\eta)}{2-d-2\eta} \right)}.\end{aligned}\tag{65}$$

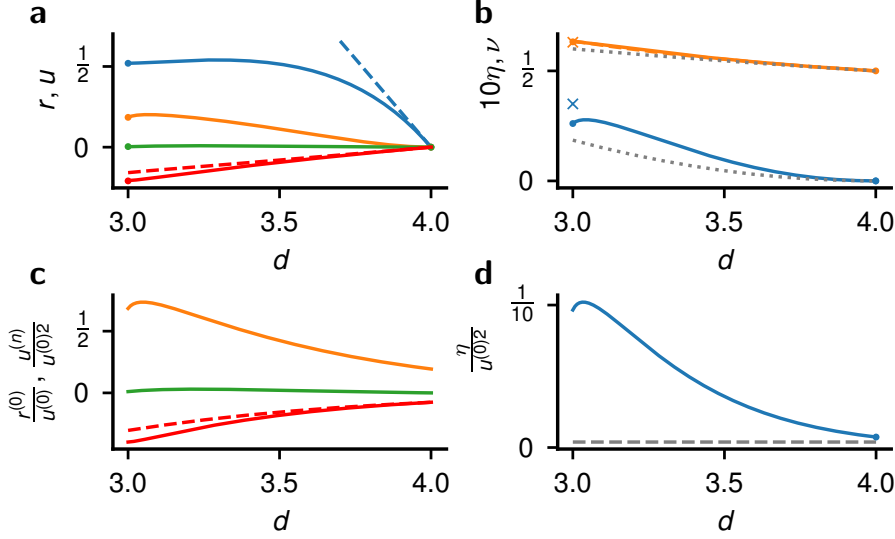


**Figure 4. Wilson-Fisher fixed point in  $\varphi^4$ -theory as function of dimension  $d \in [3, 4]$ .** **a** Fixed point as function of dimension  $d$ : i) Mass  $r_*^{(0)}$  (red solid curve, (56); red dashed curve: linear approximation in  $\epsilon = 4 - d$ ; only first line of (56)) ii) Momentum-independent interaction  $u_*^{(0)}$  (blue curve, (50); limits  $d \rightarrow 3, 4$  (51) blue dot and blue dashed line). iii) First-order momentum-dependence  $u_*^{(1)}$  (orange curve (52) and (50); orange dot: limit  $d \rightarrow 3$  (53)). iv) Second-order momentum-dependence  $u_*^{(2)}$  (green curve, (54) and (50); green dot: limit  $d \rightarrow 3$  (55)). **b** Critical exponents  $\nu$  and  $\eta$  as function of dimension  $d$ : i) Anomalous dimension  $10\eta$  (blue curve, positive root of (60); blue dots: limit  $d \rightarrow 3$  (64) and  $d \rightarrow 4$ ,  $\eta = 0$ ). ii) Critical exponent  $\nu$  (orange curve: (65); orange dots: limits  $d \rightarrow 3, 4$  (66)). Lowest order approximations of  $\epsilon$ -expansion (dashed curves (67) for  $\eta$  and  $\nu = \left(2 - (4 - d)/3\right)^{-1}$  for  $d = 4 - \epsilon$ ). **c** Coupling constants relative to interaction: i) Relative mass  $r^{(0)}/u^{(0)}$  (red curve (57); dashed curve showing only linear dependent part on  $u^{(0)}$ , first line in (57)). ii) Relative interaction  $u^{(1)}/(u^{(0)})^2$  (orange curve (52)) and  $u^{(2)}/(u^{(0)})^2$  (green curve (52)). Literature values of order 5  $\epsilon$ -expansion for  $\eta$  (blue cross;  $\eta = 0.035$  [3, p. 626] and  $\nu$  ( $\nu = 0.631(2)$  [3, p. 635]). **d** Relative anomalous dimension  $\eta/(u^{(0)})^2$  (blue curve, (59); blue dot: limit for  $d \rightarrow 4$  (61)  $\eta/(u_*^{(0)})^2 = 9/(4\pi^5) \simeq 0.0074$ ). Limit for  $d \rightarrow 4$  of classical  $\epsilon$  expansion to order  $\epsilon^2$  (gray dashed line, (63)  $\eta/(u_*^{(0)})^2 = 9/(24\pi^4) \simeq 0.0038$ ).

So for  $d = 3$  and  $d = 4 - \epsilon$  we obtain

$$\nu = \begin{cases} \frac{1}{2 - \eta + \frac{1}{6}(1 - 2\eta) \left( -\frac{5}{2} + \eta - \eta \frac{1}{3} \frac{(1 - 3\eta)(1 - 2\eta)}{1 + 2\eta} \right)} & d = 3 \\ \frac{1}{2 - \frac{1}{3}\epsilon - \frac{8}{27\pi} \epsilon^2 + \mathcal{O}(\epsilon^3)} & d = 4 - \epsilon \end{cases} \quad (66)$$

For the approximation for  $d = 4 - \epsilon$  we neglected  $\eta \propto \epsilon^2$  throughout.

exponent	$\epsilon$ -expansion $\mathcal{O}(\epsilon)$	$\epsilon$ -expansion $\mathcal{O}(\epsilon^2)$	this method	best approx.
$\nu$	0.583	0.627	0.632	0.631(2)
$\eta$	0	0.0185	0.026	0.035(3)

**Table 1. Critical exponents in  $d = 3$  dimensions.** Comparison of this method to known approximations. Best reference approximation from [3, p. 635] and [3, p. 626].

### 3. Summary and discussion

#### *Summary of quantitative results for the $\varphi^4$ -theory*

A summary of the derived expressions for the fixed point values of the mass  $r^{(0)}$ , and the momentum-dependent interaction  $\{u^{(0)}, u^{(1)}, u^{(2)}\}$  is shown in Figure 4a for  $d \in [3, 4]$ .

Critical exponents  $\nu$  and  $\eta$  as functions of the dimension are shown in Figure 4b. For  $d = 3$ , the obtained critical exponent  $\nu \simeq 0.632$  compares well to the result of an order five  $\epsilon$ -expansion  $\nu \simeq 0.631(2)$  [3, p. 635]. It is better than the result from the momentum-scale expansion for the effective action ( $\nu = 0.532$ ) [14] and to the second order  $\epsilon$ -expansion ( $\nu = 0.627$ ). The increase in accuracy is despite the observation that the quadratic momentum dependence  $\mathcal{O}(k^2)$  of the interaction vertex remains small for all dimensions  $d \in [3, 4]$  (Figure 4c).

Also the critical exponent  $\eta \simeq 0.026$  is not too far from the result of the order five  $\epsilon$ -expansion of  $\eta = 0.035(3)$ , estimated from the divergent series in powers of  $\epsilon$ . The here obtained value is closer to the true value than the two loop result of  $\eta \simeq 1/54 \simeq 0.0185$  [3, p. 625 eq. 28.7]. This is so despite the simplicity of the computation presented here, which only requires elementary one-loop integrals. Compared to the momentum-scale expansion of the effective action [14, p. 494] ( $\eta = 0.0225$ ), the improvement in accuracy is only small.

The fixed point values in a Gell-Mann-Low theory, a theory with a single marginal variable, can entirely be expressed in terms of this single marginal variable [12, Section V]. This is the basis of a renormalizable theory, where only a single renormalized coupling constant must be fixed. Correspondingly, the resulting expressions for the mass and for the momentum-dependent part of the interaction can be expressed in terms of the momentum-independent part of the interaction,  $u^{(0)}$ . Mass and the momentum-dependent part of the interaction relative to  $u^{(0)}$  (for the mass) or relative to  $(u^{(0)})^2$  (for both interaction terms) are shown in Figure 4c.

#### *Relation to earlier work*

Even though the numerical values for the anomalous dimension  $\eta$  obtained by the here-presented method and by an  $\epsilon$ -expansion of second order are not so far apart, expressing the anomalous dimension relative to  $(u^{(0)})^2$  shows that the two methods are in fact quite different: The  $\epsilon$ -expansion, to second order, yields [23, 3, p. 625 eq. 28.7]

$$\eta = \frac{1}{54}\epsilon^2 + \mathcal{O}(\epsilon^3) \quad (67)$$



and thus, with the leading order behavior of  $u^{(0)} = \pi^2 \frac{2}{3} \epsilon + \mathcal{O}(\epsilon^2)$  (Figure 4a), a ratio independent of  $\epsilon$  and thus  $d$

$$\frac{\eta}{(u^{(0)})^2} = \frac{9}{24 \pi^4}.$$

The here-proposed method instead yields a saturating form of  $u^{(0)}$  as the dimension is lowered from  $d = 4$  to  $d = 3$  (Figure 4a), while the relative quantity  $\eta/(u^{(0)})^2$  increases as  $d$  is lowered. Thus, the anomalous dimension, expressed in relation to the renormalized coupling constant, is much larger in the here-proposed method for  $d = 3$ , as shown in Figure 4d.

*Relation to the work by Wegner & Houghton [13]* The method proposed here is practically identical to the exact equations derived by Wegner & Houghton [13]. The first main contribution of the current manuscript is the presentation of an alternative derivation without using the projector formulation and the discussion how the momentum dependence of vertices leads to a tower of coupled one-loop diagrams, that we show are of identical structure as the known one-loop fluctuation expansion and the vertex expansion of the Wetterich equation. The second contribution is to demonstrate that this approach can in fact be combined with a momentum-scale expansion to obtain quantitatively accurate results in a non-perturbative setting far off the upper critical dimension.

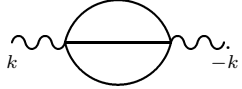
It must be noted that the computation to order  $\epsilon^2$  of the anomalous dimension performed by Wegner and Houghton yields a different result than found here. The cause of this difference is the step from eq. (3.13) to eq. (3.16) in their work: Here the authors approximately solve the set of their differential equations (3.9) - (3.12). In doing so, they insert the contribution of the tree-diagrams of the form (28) contributing to the six-point vertex  $v_6$  given by their eq. (3.12) into the second line of their eq. (3.11). What they thus implicitly assume is that the six-point vertex  $v_6$  is produced within the same decimation shell as the one integrated out in the flow of  $v_4$ . This, however, is only true for vanishing external momenta. Stated differently, they neglect that, for non-zero external momenta  $k$  of their four point vertex  $v_4(k)$ , the two propagator lines in the composed diagram of the form (31) necessarily belong to different decimation shells. The propagator line that connects the two four point vertices in their eq. (3.12) of  $v_6$ , as a consequence, stems from a different decimation shell than the propagator in their eq. (3.11). Our calculation takes this momentum-dependence into account. This results in the factor  $\left(\frac{\ell_j}{\ell_i}\right)^{6-3\eta-2d}$  in front of  $S_{\ell_i}^{(6)}\left(\frac{\ell_i}{\ell_j}\{k\}\right)$  in (34), which is missing in Wegner & Houghton's approximate solution, their eq. (3.16). This additional approximation they make yields a result for the critical exponent  $\eta$  that, to order  $\epsilon^2$ , is identical to the known two-loop result. A careful interpretation of their equations in fact yields the same result as presented in the current manuscript, had they taken seriously the rescaling term  $(6 - 3\eta - 2d)v_6$  in their eq. (3.12) in conjunction with the momentum dependence, as explained in Figure 2.

A closely related approach is the functional renormalization group [15, 24] for the effective action, the first Legendre transform of the free energy. Employing a hard cutoff, this method has been used previously to compute the momentum dependence of the self-energy in weakly interacting Bosons [17, 18]. Here as well, a momentum-scale expansion of the interaction leads to a non-differentiable momentum

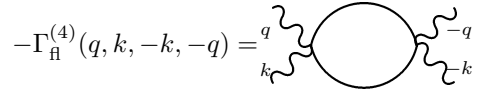
dependence  $\propto \|k\|$  of the interaction vertex that enters the computation of the anomalous dimension (cf. i.p. [18] eq. (11)) and that becomes marginal in  $d = 3$  dimensions, as in the present manuscript (cf. eq. (44)).

*Relation to the  $\epsilon$ -expansion* An important cross check of the method is its compatibility with previous methods, foremost the established  $\epsilon$ -expansion [23, 11, 12]. The interaction  $u_*^{(0)} \simeq \pi^2 \frac{2}{9} \epsilon + \mathcal{O}(\epsilon^2)$ , given by (51), is in fact identical to order  $\mathcal{O}(\epsilon)$  in the two approaches. Also, the momentum dependence only arises at order  $\mathcal{O}(\epsilon^2)$ , given by (53) and (55), again in line with the  $\epsilon$ -expansion. A qualitative difference is, though, that the leading order  $\mathcal{O}(\epsilon^2)$  momentum-dependence of the interaction vertex here is  $\propto u_*^{(1)} \|k_1 + k_2\|$  with  $\Lambda^{d-3} u_*^{(1)} \simeq \frac{8\pi}{27} \epsilon^2 + \mathcal{O}(\epsilon^3)$ , whereas the quadratic momentum-dependence  $\propto u_*^{(2)} (k_1 + k_2)^2$  only arises at the next order in  $\epsilon$ , namely  $\Lambda^{d-2} u_*^{(2)} \simeq \frac{\pi^2}{72} \epsilon^3 + \mathcal{O}(\epsilon^4)$ . The correction to  $\eta$  to order  $\mathcal{O}(\epsilon^2)$  comes from the third line of the self-energy correction (46) by inserting the momentum-dependence  $\propto u_*^{(1)}$  in the middle term of (47).

Such contribution  $\propto u_*^{(1)}$  is not present in the classical second order  $\epsilon$ -expansion, because this method treats the momentum dependence of the interaction differently. The leading order  $k$ -dependence of the self-energy in the  $\epsilon$ -expansion comes from the diagram (cf. [11, Fig 5.4])


(68)

The  $k$ -dependence of this diagram results from an expansion in the external momentum  $k$ . This diagram can also be seen as arising from contracting a pair of legs of the one-loop fluctuation correction to the four point vertex,  $\Gamma_{\text{fl}}^{(4)}$ , as in eq. (46). This sub-diagram of (68) is of the form


(69)

where  $q$  is the momentum of integration of the upper loop in (68). The dependence on  $k$  then results from the algebraic form of the diagram

$$-\Gamma_{\text{fl}}^{(4)}(q, k, -k, -q) \propto \int \frac{dk'}{(2\pi)^d} \frac{u_0^2}{(r_0 + (q + k')^2)(r_0 + (k - k')^2)}, \quad (70)$$

when expanding to quadratic order in  $k$ : One obtains only spherically symmetric diagrams  $\propto k^2$  and uniaxial diagrams  $\int dk' (k \cdot k')^2 \propto k^2$ ; to lowest order in  $k$  one thus obtains a dependence  $\propto k^2$ . In particular, there is no dependence  $\propto \|k\|$  arising in the perturbative approach, because expanding for small  $k$ , terms  $\propto \int dk' (k \cdot k')$  vanish by the point-symmetry of the integrand. In contrast, in our approach we have found this very term  $\propto u_*^{(1)} \|k\|$  to produce the dominant contribution to  $\eta$ .

What is the reason for this qualitative difference between the two approaches? The non-differentiable momentum dependence  $\propto u_*^{(1)} \|k\|$  of the interaction in our approach comes about by the fact that a fluctuation correction of the form (69) at scale  $\ell$  necessarily must have one of the propagator lines above the current cutoff  $|q + k'| > \Lambda_\ell$  or  $|k - k'| > \Lambda_\ell$ . When expanded for small momenta, this leads to integrals of the form  $\propto \int dk' (k \cdot k') \theta(k \cdot k') \propto \|k\|$ , where  $\theta(k \cdot k')$  constrains the

integration to half the momentum shell. These contributions thus do not vanish, as opposed to the perturbative approach, where one integrates over full momentum shells.

On a more abstract level, we can summarize these observations as follows. The infinitesimal Wilsonian RG studied here leads to a functional differential equation of the form

$$\ell \frac{dS_\ell}{d\ell} = \beta\{S_\ell\}, \quad (71)$$

where  $\beta : \mathcal{F} \mapsto \mathcal{F}$  is a mapping from the space of functionals  $\mathcal{F} := \{f|f : \mathcal{C} \mapsto \mathbb{R}\}$  into itself, where  $\mathcal{C}$  is the space of functions, in our case the configurations  $\varphi$  of our system. In the chosen Fourier representation of  $\varphi$ , the functional mapping  $\beta$  may thus couple different  $k$ -vectors. This is in fact the case, as we illustrate in [Figure 2](#): The flow for the Taylor coefficient  $S_\ell^{(4)}(q_1, q_2, q'_1, q'_2)$  of  $S_\ell$  depends on the Taylor coefficient  $S_\ell^{(6)}(q_1, q_2, q_3, \dots)$ ; here  $S_\ell^{(4)}$  appears on the left hand side of (71) and  $S_\ell^{(6)}$  on the right hand side. The here-followed approach takes this functional seriously; as a result, the value  $S_\ell^{(6)}$  that appears on the right hand side of (71) depends on the momentum  $q_1 + q_2 + q_3$  given by the arguments  $q_1$  and  $q_2$  of  $S_\ell^{(4)}$  and the loop momentum  $q_3$ , because the decimation step  $\ell_i(q_1 + q_2 + q_3)$  in which  $S_\ell^{(6)}$  has been produced is a function of this very momentum, as explained in [Section 2.8](#).

This is what appears to us being neglected in the perturbative approach of the  $\epsilon$ -expansion: Here, the diagram (70) is composed of vertices  $u_0$  and propagators  $(r_0 + k^2)^{-1}$ , all of which take the values of the current decimation step; the perturbative calculation thus neglects the fact that each propagator line necessarily belongs to a single decimation step that integrates out the degrees of freedom at the very momentum that is carried by the propagator.

The difference between the perturbative calculation and our approach consequently shows up only in the flow of vertices at non-zero external momenta; the value for  $u_0$  at vanishing momentum to order  $\epsilon$  is identical. In contrast, the two methods yield quantitatively different results for the anomalous dimension, because this quantity is defined in terms of the momentum dependence of the self-energy.

The estimate of the anomalous dimension by the  $\epsilon$ -expansion, to quadratic order  $\mathcal{O}(\epsilon^2)$ , is roughly by about a factor 2 smaller than the estimate of a high temperature expansion, as already noted in Fig. 1 of [\[23\]](#). In their ref 16, the authors point out that their estimate is in fact too small. Also the comment after eq. (8.29) on p. 137 of [\[11\]](#) points out that the result of the  $\epsilon$ -expansion at second order is too small by about a factor of 2. Our estimate is larger by a factor  $6/\pi \simeq 1.9$  than the  $\epsilon$ -expansion at second order. The here-presented method is thus in better agreement with the high temperature expansion and with higher orders of the  $\epsilon$ -expansion. However, the approximations made here, truncating the vertex expansion and expanding in small momenta, requires further careful analysis to see if this improvement is truly systematic.

On the technical side a difference of the proposed method is that it does not require resummation of a divergent series, as opposed to the  $\epsilon$ -expansion. The flow equations expose the desired quantities simply by their fixed point values. This shows the non-perturbative nature of the method. The approximation made here is not in the number of loops – we have shown above that the one-loop calculation is exact; this is simply a result of the phase space volume contributing to an infinitesimal marginalization step being proportional to the (infinitesimal) thickness of the momentum shell times the number of loops. Formally, this result is thus in line with

exact functional RG equations [13, 15, 24], where also only single-loop integrals are required. For the functional RG of the effective action [15, 24], similar approximations, a momentum scale expansion combined with the vertex expansion, have been applied to investigate critical behavior of weakly interacting Bosons and in particular to obtain an approximation of the momentum dependence of the self-energy and thus the anomalous dimension [17, 18].

In the simple example shown here we did not compute the flow of the six-point vertex. At  $d = 3$ , however, the six point vertex becomes marginal so that its contribution can potentially become substantial. Since the  $|k|$ -momentum-dependence of the six point vertex is less relevant by one power of  $\ell$ , an approximation taking the momentum-independent part into account is still simple and yields potentially better results. Also, taking into account the momentum dependence of the four-point vertex in computing its own corrections is expected to improve the results close to  $d = 3$ .

### 3.1. Conclusion and outlook

We here analyzed the exact Wegner-Houghton renormalization group equation, here derived as an infinitesimal momentum-shell Wilsonian RG. A vertex expansion exposes the close relation to the Wetterich RG with hard cutoff. We found that the flow equations can successfully be closed by combining the vertex expansion with a momentum-scale approximation. For the scalar  $\varphi^4$ -theory, one obtains a highly accurate approximation for  $\nu$  and a reasonable accurate approximation for  $\eta$ ; even though, the latter vanishes at one-loop order of the orthodox  $\epsilon$ -expansion.

Our main motivation is to render a more complete picture on the relation between the Wegner-Houghton RG and the Wilson RG and  $\epsilon$ -expansion as well as the Wetterich RG; in particular, to point out where approximations are being made. The main result is a tower of coupled flow equations for the momentum-dependent vertices that is logically consistent with a continuous marginalization of modes.

The obvious weakness of the here-presented solution of this set of equations is the requirement of truncating the vertex expansion and the treatment of the momentum dependence; in both points one faces basically the same problem as in the vertex expansion of the Wetterich RG. Even though resummation techniques in  $\epsilon = d_c - d$  are not required here (neither in the Wetterich RG), which may a priori be regarded as an advantage, there is of course a large body of literature that has carefully studied the behavior of these asymptotic series. More work is needed to thoroughly study the limits of the vertex expansion combined with the momentum-scale approximation used here.

The use of the renormalization group to study phenomena that arise from the interaction of processes on many different scales is not restricted to systems from the core domains of physics. Our motivation to employ the renormalization group, for example, arises from the wish to understand how activity organizes in neuronal systems. Field theoretical formulations of neuronal networks have begun to be employed in this field (see e.g. [25, 26, 21] for reviews). One here knows the dynamical equations on the microscopic level, namely for individual neurons, but experiments often only yield coarse-grained signals, such as the local-field potential [27]. Moreover, there is experimental evidence that neuronal systems may operate at critical points [28]. Methods from statistical physics are therefore commonly employed in this field; often from equilibrium statistical mechanics. For example the pairwise maximum-

entropy model [29], the Ising model, is fitted to binned neuronal activity data [30]. More recent developments have formulated neuronal systems as a Ginzburg-Landau field theory, a genuine non-equilibrium formulation [31]. Such systems bear strong similarity to the Kardar-Parisi-Zhang model [8]. For the latter model it is known that the momentum dependence of the self-energy is a key ingredient of the flow equations. Such models thus necessitate efficient approximations of the momentum dependence, as investigated here. But not only the study of coarse-graining and critical dynamics in biological neuronal networks requires renormalization group techniques. Also the transformations performed by deep artificial neuronal networks are composed of concatenations of large numbers of relatively simple transformations by each layer. Addressing the question how representations of data arise in these networks [32] may therefore also be studied by renormalization group methods [33]. Applying an established technique to a new field, often shows a method in a new light. This is how the question of the momentum dependence in the Wilson RG, as discussed by the current manuscript, arose in the present case.

We hope that the here presented method may become fruitful to obtain simple and intuitive diagrammatic approximations for critical phenomena in various systems that so far required more elaborate non-perturbative methods. We also hope that the partly pedagogical presentation may be helpful for the accessibility by a broad readership.

#### 4. Acknowledgments

We are grateful to the comments by Peter Kopietz on an earlier version of this manuscript. These comments in particular considerably improved the discussion of the presented work to the  $\epsilon$ -expansion and to non-perturbative techniques using the functional RG and the momentum-scale expansion. We also thank the anonymous reviewer for the helpful and constructive critique and for pointing out the common misunderstanding that the field-theoretical RG is only applicable to renormalizable field theories. We would further like to acknowledge helpful discussions with Tobias Kuehn, and Kirsten Fischer that lead to the initial question on the momentum-dependence of the infinitesimal RG.

This work was partially supported by the European Union’s Horizon 2020 research and innovation programme under grant agreement No. 785907 (Human Brain Project SGA2), the Exploratory Research Space (ERS) seed fund G:(DE-82)EXS-SF-neuroIC002, and the German Federal Ministry for Education and Research (BMBF Grant 01IS19077A).

#### 5. Appendix

##### 5.1. Gaussian part of the action

Before proceeding to the general problem to apply the coarse-graining defined in Section 2.2 to the full action, consider the quadratic term which is

$$S_0[\varphi] := -\frac{1}{2} \int_k \varphi(-k) (r^{(0)} + r^{(2)} k^2) \varphi(k) = : -\frac{1}{2} \varphi^T G^{-1} \varphi, \quad (72)$$

where we introduce a matrix-vector notation and define

$$G^{-1}(k, k') = \delta(k + k') (r^{(0)} + r^{(2)} k^2).$$

This matrix is diagonal in the sense that it only couples the component  $\varphi(k)$  with  $\varphi(-k)$ .

To perform the marginalization step (6) one needs to evaluate  $S_0[\varphi_< + \varphi_>]$

$$\varphi^T G^{-1} \varphi = (\varphi_< + \varphi_>)^T G^{-1} (\varphi_< + \varphi_>). \quad (73)$$

As  $G^{-1}$  is diagonal in frequency domain, it couples only frequencies  $0 < |q| < \Lambda \ell^{-1}$  among another and frequencies  $\Lambda \ell := \Lambda \ell^{-1} < |k| < \Lambda$  among another, but it does not couple  $q$  and  $k$ ; cross terms in multiplying out (73) are thus dropped to get

$$\begin{aligned} \varphi^T G^{-1} \varphi &= \varphi_<^T G^{-1} \varphi_< \\ &+ \varphi_>^T G^{-1} \varphi_>. \end{aligned} \quad (74)$$

The decimation step in (6) thus only affects the term in the second line of (74), which yields

$$\begin{aligned} \mathcal{Z}_> &:= \int \mathcal{D}\varphi_> \exp\left(-\frac{1}{2} \varphi_>^T G^{-1} \varphi_>\right) \\ &= \prod_{\Lambda \ell < |k| < \Lambda} (2\pi G(k))^{\frac{1}{2}} \\ \ln \mathcal{Z}_> &= \frac{1}{2} \int_{\Lambda \ell < |k| < \Lambda} \ln 2\pi G(k). \end{aligned} \quad (75)$$

This contribution is hence a multiplicative factor  $\mathcal{Z}_>$  changing the partition function, independent of  $\varphi_<$ . Thus it affects the free energy. But it has no consequence on the correlation functions of the field, because it becomes an additive correction to the cumulant-generating functional  $W = \ln \mathcal{Z}$ . Since we here want to calculate only the critical exponents, we will neglect this term.

The remaining part of the coarse-grained action stems from the first line in (74), which just yields

$$\exp\left(-\frac{1}{2} \varphi_<^T G^{-1} \varphi_<\right).$$

So together the coarse-grained action is

$$\begin{aligned} S_\ell[\varphi_<] &= \ln \left( \mathcal{Z}_> \exp\left(-\frac{1}{2} \varphi_<^T G^{-1} \varphi_<\right) \right) \\ &= \ln \mathcal{Z}_> - \frac{1}{2} \varphi_<^T G^{-1} \varphi_<. \end{aligned} \quad (76)$$

The last line shows that the rescaled action, apart from the inconsequential constant, is the same as the original one (72). With one exception: the momenta of the fields only extend up to  $\Lambda \ell^{-1}$  instead of  $\Lambda$ .

### 5.2. Expansion of momentum dependence of rescaling term

The momentum dependence of the rescaling term appearing in (34), to order  $\mathcal{O}(k_\ell^2)$ , takes the form

$$\begin{aligned} \left(\frac{\ell_j}{\ell_i}\right)^{6\left(1-\frac{d+\eta}{2}\right)+d} &= \exp\left(\left[6\left(1-\frac{d+\eta}{2}\right)+d\right]\frac{1}{2}\ln\left(\frac{\ell_j}{\ell_i}\right)^2\right) \\ &= \exp\left(\left[6\left(1-\frac{d+\eta}{2}\right)+d\right]\frac{1}{2}\ln\left(\frac{(k'+k)^2}{\Lambda^2}\right)\right) \end{aligned} \quad (77)$$

$$\begin{aligned}
 &= \exp \left( \left[ 6 \left( 1 - \frac{d+\eta}{2} \right) + d \right] \frac{1}{2} \ln \left( \frac{\overbrace{k'^2}^{\Lambda^2} + 2k' \cdot k + k^2}{\Lambda^2} \right) \right) \\
 &= \exp \left( \left[ 6 \left( 1 - \frac{d+\eta}{2} \right) + d \right] \frac{1}{2} \ln \left( 1 + \frac{2k' \cdot k + k^2}{\Lambda^2} \right) \right) \\
 &\simeq \exp \left( \left[ 6 \left( 1 - \frac{d+\eta}{2} \right) + d \right] \left( \frac{1}{2} \frac{2k' \cdot k + k^2}{\Lambda^2} - \frac{1}{2} \frac{1}{2} \frac{4(k' \cdot k)^2}{\Lambda^4} \right) + \mathcal{O}(k^3) \right) \\
 &\simeq 1 + \left[ 6 \left( 1 - \frac{d+\eta}{2} \right) + d \right] \left( \frac{2k' \cdot k + k^2}{2\Lambda^2} - \frac{(k' \cdot k)^2}{\Lambda^4} \right) \\
 &\quad + \frac{1}{2!} \left[ 6 \left( 1 - \frac{d+\eta}{2} \right) + d \right]^2 \frac{(k' \cdot k)^2}{\Lambda^4} + \mathcal{O}(k^3) \\
 &= 1 \\
 &\quad + \frac{(k' \cdot k)}{\Lambda^2} \left( 6 \left( 1 - \frac{d+\eta}{2} \right) + d \right) \\
 &\quad + \frac{k^2}{2\Lambda^2} \left( 6 \left( 1 - \frac{d+\eta}{2} \right) + d \right) \\
 &\quad + \frac{(k' \cdot k)^2}{\Lambda^4} \left[ \frac{1}{2} \left( 6 \left( 1 - \frac{d+\eta}{2} \right) + d \right)^2 - \left( 6 \left( 1 - \frac{d+\eta}{2} \right) + d \right) \right] \\
 &= 1 + \left( 6 - 2d - 3\eta \right) \left( \frac{(k' \cdot k)}{\Lambda^2} + \frac{k^2}{2\Lambda^2} + \frac{(k' \cdot k)^2}{\Lambda^4} \left[ 2 - d - \frac{3}{2}\eta \right] \right).
 \end{aligned}$$

### 5.3. Uniaxial and spherical symmetric integrals

We write for short

$$\int d\Omega f(\Omega \cdot \Lambda) \equiv \int_{|k|=\Lambda} f(k).$$

If the integrand is spherically symmetric, so that it does not depend on  $\Omega$ , we may perform the angular integral to obtain

$$\int d\Omega = S_d = \frac{2\pi^{\frac{d}{2}}}{\Gamma(\frac{d}{2})}, \quad (78)$$

which yields the area of the  $d$ -dimensional unit sphere and  $\Gamma$  denotes the gamma function  $\Gamma(z) = \int_0^\infty t^{z-1} e^{-t} dt$ .

For uniaxial integrals we have [34, p. 379]

$$\begin{aligned}
 I &= \int \frac{d^d q}{(2\pi)^d} f(|q|, \theta) \\
 &= \int dq q^{d-1} \int d\Omega f(|q|, \theta) \\
 &= \int dq q^{d-1} C \int_0^\pi d\theta (\sin \theta)^{d-2} f(|q|, \theta), \\
 C &= \frac{S_d}{(2\pi)^d} \frac{1}{\int_0^\pi d\theta (\sin \theta)^{d-2}} = \frac{S_{d-1}}{(2\pi)^d}.
 \end{aligned} \quad (79)$$

We need such integrals to compute the  $k$ -dependence of the fluctuation corrections. Here the integrand  $f(|q|, \theta)$  only depends on the absolute magnitude  $|q|$  and a single angle  $\theta$  between a specified direction in  $\mathbb{R}^d$  and the  $q$ -vector to integrate over.

We need in particular integrands of the form  $f(|q|) \cos^2(\theta)$  for which it holds that

$$\begin{aligned}
 J &= \int \frac{d^d q}{(2\pi)^d} f(|q|) \cos^2(\theta) \\
 &= \frac{1}{(2\pi)^d} \int d\Omega \cos^2(\theta) \int dq q^{d-1} f(|q|) \\
 &= \frac{S_d}{(2\pi)^d} \frac{1}{d} \int dq q^{d-1} f(|q|).
 \end{aligned} \tag{80}$$

This can be seen as follows: For the angular part of (80) alone we get with (79)

$$\begin{aligned}
 \int d\Omega \cos^2(\theta) &= C \int_0^\pi d\theta \sin^{d-2}(\theta) \cos^2(\theta) \\
 &= C \int_0^\pi d\theta \sin^{d-2}(\theta) (1 - \sin^2(\theta)) \\
 &= C \int_0^\pi d\theta \sin^{d-2}(\theta) - \sin^d(\theta).
 \end{aligned} \tag{81}$$

We may reduce the latter integral to the former for  $d > 1$

$$\begin{aligned}
 I &:= \int_0^\pi d\theta (\sin \theta)^d = \int_0^\pi d\theta \underbrace{\sin \theta}_{f'} \underbrace{(\sin \theta)^{d-1}}_g \\
 &= \underbrace{-\cos \theta (\sin \theta)^{d-1}}_0 \Big|_0^\pi + \int_0^\pi d\theta \cos^2 \theta (d-1) (\sin \theta)^{d-2} \\
 &= (d-1) \int_0^\pi d\theta (1 - \sin^2 \theta) (\sin \theta)^{d-2} \\
 &= (d-1) \int_0^\pi d\theta (\sin \theta)^{d-2} - (d-1) I.
 \end{aligned}$$

So we get

$$I = \frac{d-1}{d} \int_0^\pi d\theta (\sin \theta)^{d-2}.$$

We can therefore combine both angular integrals (81) as

$$\frac{1}{(2\pi)^d} \int d\Omega \cos^2(\theta) = \frac{S_d}{(2\pi)^d} \left(1 - \frac{d-1}{d}\right) = \frac{S_d}{(2\pi)^d} \frac{1}{d}, \tag{82}$$

from which follows (80).

#### 5.4. Momentum-dependent integral of four-point vertex

Here we compute the integral appearing in (34) at small momenta  $k$ , using (77). We hence have to compute two spherically symmetric and two uniaxial terms. The latter uniaxial term  $\propto (k' \cdot k)^2$  in (77) yields with  $(k \cdot k')^2 = \|k\|^2 \Lambda^2 \cos(\Omega_1)^2$  and (82)

$$\int_{|k'|=\Lambda} \theta(k' \cdot k) (k \cdot k')^2 = \frac{1}{2} \Lambda^2 k^2 \frac{S_d}{d}, \tag{83}$$

where the factor 1/2 comes from the constraint that by  $\theta(k' \cdot k)$  we are only integrating over half a momentum shell. The spherically symmetric integrals ( $\propto (k')^0$ ) simply



produce one factor  $S_d$ ; here the entire shell contributes for vanishing external momenta. The remaining integral is given with (79) by

$$\begin{aligned}
 & \int_{|k'|=\Lambda} \theta(k' \cdot k+) k \cdot k' & (84) \\
 &= \Lambda \|k\| \int_{|k'|=\Lambda} \theta(\cos(\Omega_1)+) \cos(\Omega_1) \\
 &\stackrel{(79)}{=} \Lambda S_{d-1} \|k\| \int_0^\pi d\Omega_1 (\sin \Omega_1)^{d-2} \theta(\cos(\Omega_1)+) \cos(\Omega_1) \\
 &= S_{d-1} \Lambda \|k\| \int_0^{\pi/2} d\Omega_1 (\sin \Omega_1)^{d-2} \cos(\Omega_1) \\
 &= S_{d-1} \Lambda \|k\| \frac{1}{d-1} (\sin \Omega_1)^{d-1} \Big|_0^{\pi/2} = \Lambda S_{d-1} \|k\| \frac{1}{d-1}.
 \end{aligned}$$

Taken together, we get (37) in the main text.

### 5.5. Momentum dependence of self-energy

Approximating the dependence on the momentum  $q$  for  $q \ll k$  up to orders of  $\mathcal{O}(q^2)$ , the resulting integrals appearing in (46) are again either spherically symmetric or uniaxial which follows with  $\sqrt{1+x} \simeq 1 + \frac{x}{2} - \frac{x^2}{8} + \mathcal{O}(x^2)$  from the expansion (38)

$$\begin{aligned}
 & \frac{1}{4!} S_\ell^{(4)}(q, k, -k, q) \\
 & \simeq u_\ell^{(0)} \\
 & + u_\ell^{(1)} \|k\| \left( 1 + \underbrace{\frac{q \cdot k}{\|k\|^2}}_{\rightarrow 0} + \frac{1}{2} \frac{q^2}{\|k\|^2} - \frac{1}{2} \frac{(q \cdot k)^2}{\|k\|^4} \right) \\
 & + u_\ell^{(2)} (q^2 + \underbrace{2q \cdot k + k^2}_{\rightarrow 0}) + \mathcal{O}\left(\frac{\|q\|^3}{\|k\|^3}\right).
 \end{aligned}$$

Taking the integral over the sphere of  $k$ -vectors in (46), the terms  $\propto 2q \cdot k$  do not contribute by their point symmetry, indicated by the underbraces. The terms  $\propto q^2$  yield a momentum dependence of the self-energy. The uniaxial term is again of the form (80) and yields

$$-\frac{u_\ell^{(1)}}{2} \int_{|k|=\Lambda_\ell} \frac{(q \cdot k)^2}{\|k\|^3} = -\frac{u_\ell^{(1)}}{2\Lambda_\ell} \frac{S_d}{d} q^2.$$

To determine the flow equations for  $r^{(0)}$  and  $r^{(2)}$ , we need to decompose the self-energy corrections  $\ell \frac{d}{d\ell} S_\ell^{(2)}(q, -q)$  according to their  $q^2$ -dependence as

$$\begin{aligned}
 \ell \frac{d}{d\ell} r_\ell^{(0)} &= -\ell \frac{d}{d\ell} S_\ell^{(2)}(0, 0), & (85) \\
 \ell \frac{d}{d\ell} r_\ell^{(2)} &= -\lim_{q \rightarrow 0} \frac{\ell \frac{d}{d\ell} S_\ell^{(2)}(q, -q) - \ell \frac{d}{d\ell} S_\ell^{(2)}(0, 0)}{q^2}.
 \end{aligned}$$

It is therefore sufficient to compute (46) for small momenta  $q$ . This, in turn, means we need the  $q$ -dependence of the interaction vertex in the first two entries, given by (38).

The projections (85) hence yield the flow equation for the momentum-independent parameter

$$\begin{aligned} \ell \frac{d}{d\ell} r_\ell^{(0)} &= 2 \cdot 2 \cdot \frac{\Lambda^d}{(2\pi)^d} \cdot \int_{|k|=\Lambda} u_\ell^{(0)} G_\ell(k) \\ &+ 2 \cdot 4 \cdot \frac{\Lambda^d}{(2\pi)^d} \cdot \int_{|k|=\Lambda} (u_\ell^{(0)} + u_\ell^{(1)} \|k\| + u_\ell^{(2)} k^2) G_\ell(k) \\ &= 2 \cdot \frac{S_d \Lambda^d}{(2\pi)^d} \cdot \frac{6 u_\ell^{(0)} + 4 u_\ell^{(1)} \Lambda + 4 u_\ell^{(2)} \Lambda^2}{r_\ell^{(0)} + r_\ell^{(2)} \Lambda^2}. \end{aligned}$$

The flow of the momentum-dependent term of the self-energy then follows from (46), (47), and (85) as

$$\begin{aligned} \ell \frac{d}{d\ell} r_\ell^{(2)} &= 2 \cdot 4 \cdot \frac{\Lambda^d}{(2\pi)^d} \cdot \int_{|k|=\Lambda} \left( \frac{u_\ell^{(1)}}{2\Lambda} \left(1 - \frac{1}{d}\right) + u_\ell^{(2)} \right) G_\ell(k). \\ &= 8 \cdot \frac{S_d \Lambda^d}{(2\pi)^d} \cdot \frac{\frac{u_\ell^{(1)}}{2\Lambda} \left(1 - \frac{1}{d}\right) + u_\ell^{(2)}}{r_\ell^{(0)} + r_\ell^{(2)} \Lambda^2}. \end{aligned}$$

### 5.6. Detailed calculation of fixed points and critical exponents for $3 \leq d \leq 4$

We may now compute the values of the fixed point for arbitrary dimensions between 3 and 4. We again determine  $\eta$  such that  $r_*^{(2)} \equiv 1$ .

*Interaction  $u$*  The fixed point for the momentum-independent four point coupling must obey  $0 \stackrel{!}{=} du_\ell^{(0)}/d\ell$  from which follows with (43)

$$\begin{aligned} 0 &= (4 - d - 2\eta) u_*^{(0)} - 36 \cdot \frac{S_d \Lambda^d}{(2\pi)^d} \cdot \frac{(u_*^{(0)})^2}{(r_\ell^{(0)} + \Lambda^2)^2} \\ r_*^{(0)} \ll \Lambda^2 &\simeq (4 - d - 2\eta) u_*^{(0)} - 36 \cdot \frac{S_d \Lambda^{d-4}}{(2\pi)^d} \cdot (u_*^{(0)})^2 \\ \Lambda^{d-4} u_*^{(0)} &\simeq (2\pi)^d \frac{4 - d - 2\eta}{36 S_d}. \end{aligned} \tag{86}$$

The first-order momentum dependence becomes with  $0 \stackrel{!}{=} du_\ell^{(1)}/d\ell$  and (44)

$$\begin{aligned} 0 &= (3 - d - 2\eta) u_*^{(1)} - 36 \left(2(3 - d) - 3\eta\right) \frac{S_{d-1}}{d-1} \frac{\Lambda^d}{(2\pi)^d} \frac{(u_*^{(0)})^2}{(r_\ell^{(0)} + \Lambda^2)^2} \frac{1}{\Lambda} \\ r_*^{(0)} \ll \Lambda^2 &\simeq (3 - d - 2\eta) u_*^{(1)} - 36 \left(2(3 - d) - 3\eta\right) \frac{S_{d-1}}{d-1} \frac{\Lambda^{d-5}}{(2\pi)^d} (u_*^{(0)})^2 \\ u_*^{(1)} &\simeq 36 \frac{2(3 - d) - 3\eta}{3 - d - 2\eta} \frac{S_{d-1}}{d-1} \frac{\Lambda^{d-5}}{(2\pi)^d} (u_*^{(0)})^2 \\ \Lambda^{d-3} u_*^{(1)} &\simeq \frac{(2\pi)^d}{36} \frac{2(3 - d) - 3\eta}{3 - d - 2\eta} (4 - d - 2\eta)^2 \frac{S_{d-1}}{(d-1) S_d^2}. \end{aligned} \tag{87}$$

The quadratic momentum dependence of the interaction with  $0 \stackrel{!}{=} du_\ell^{(2)}/d\ell$  and (45)

$$\begin{aligned}
 0 &= (2-d-2\eta) u_*^{(2)} - 36 \left( 2(3-d) - 3\eta \right) \frac{4-d-3\eta}{4d} \frac{S_d \Lambda^d}{(2\pi)^d} \frac{(u_*^{(0)})^2}{(r_*^{(0)} + \Lambda^2)^2} \frac{1}{\Lambda^2} \\
 &\stackrel{r_*^{(0)} \ll \Lambda^2}{\simeq} (2-d-2\eta) u_*^{(2)} - 36 \left( 2(3-d) - 3\eta \right) \frac{4-d-3\eta}{4d} \frac{S_d \Lambda^{d-6}}{(2\pi)^d} (u_*^{(0)})^2 \\
 u_*^{(2)} &\simeq 36 \frac{2(3-d) - 3\eta}{2-d-2\eta} \frac{4-d-3\eta}{4d} \frac{S_d \Lambda^{d-6}}{(2\pi)^d} (u_*^{(0)})^2 \\
 \Lambda^{d-2} u_*^{(2)} &\simeq \frac{(2\pi)^d}{36 S_d} \frac{2(3-d) - 3\eta}{2-d-2\eta} \frac{(4-d-3\eta)(4-d-2\eta)^2}{4d}. \tag{88}
 \end{aligned}$$

*Mass  $r$*  To value for  $r_*^{(0)}$ , in the approximation  $r_*^{(0)} \ll \Lambda^2$ , is determined from  $0 \stackrel{!}{=} dr_\ell^{(0)}/d\ell$  and (48)

$$\begin{aligned}
 0 &= (2-\eta) r_*^{(0)} + 2 \cdot \frac{S_d \Lambda^d}{(2\pi)^d} \cdot \frac{6 u_*^{(0)} + 4 u_*^{(1)} \Lambda + 4 u_*^{(2)} \Lambda^2}{r_*^{(0)} + \Lambda^2} \\
 &\stackrel{r_*^{(0)} \ll \Lambda^2, \eta \ll 2}{\simeq} 2 r_*^{(0)} + 2 \cdot \Lambda^2 \frac{S_d \Lambda^{d-4}}{(2\pi)^d} \cdot \left( 6 u_*^{(0)} + 4 u_*^{(1)} \Lambda + 4 u_*^{(2)} \Lambda^2 \right) \\
 \Lambda^{-2} r_*^{(0)} &\simeq - \frac{S_d}{(2\pi)^d} \cdot \left( 6 \Lambda^{d-4} u_*^{(0)} + 4 \Lambda^{d-3} u_*^{(1)} + 4 \Lambda^{d-2} u_*^{(2)} \right) \\
 &\simeq - \frac{6 S_d}{(2\pi)^d} \cdot \Lambda^{d-4} u_*^{(0)} \\
 &\quad - \frac{144 S_d}{(2\pi)^{2d}} \frac{2(3-d) - 3\eta}{3-d-2\eta} \left( \frac{S_{d-1}}{d-1} + \frac{4-d-3\eta}{4d} S_d \right) (\Lambda^{d-4} u_*^{(0)})^2. \tag{89}
 \end{aligned}$$

*Critical exponent  $\eta$*  Demanding  $0 \stackrel{!}{=} dr_\ell^{(2)}/d\ell$  the anomalous dimension  $\eta$  is determined from (49) as

$$\begin{aligned}
 \eta &= 8 \frac{S_d \Lambda^d}{(2\pi)^d} \cdot \frac{\frac{u_*^{(1)}}{2\Lambda} \left( 1 - \frac{1}{d} \right) + u_*^{(2)}}{r_*^{(0)} + \Lambda^2} \\
 &\stackrel{r_*^{(0)} \ll \Lambda^2}{\simeq} 8 \frac{S_d \Lambda^{d-2}}{(2\pi)^d} \cdot \left( \frac{u_*^{(1)}}{2\Lambda} \left( 1 - \frac{1}{d} \right) + u_*^{(2)} \right). \tag{90}
 \end{aligned}$$

Inserting (50), (52), and (54), we get

$$\begin{aligned}
 \eta &\simeq 8 \frac{S_d}{(2\pi)^d} \cdot \left( \frac{1}{2} \left( 1 - \frac{1}{d} \right) \Lambda^{d-3} u_*^{(1)} + \Lambda^{d-2} u_*^{(2)} \right) \\
 &= 8 \frac{S_d}{(2\pi)^{2d}} \cdot \left( \frac{1}{2} \left( 1 - \frac{1}{d} \right) 36 \frac{2(3-d) - 3\eta}{3-d-2\eta} \frac{S_{d-1}}{d-1} \right. \\
 &\quad \left. + 36 \frac{2(3-d) - 3\eta}{2-d-2\eta} \frac{4-d-3\eta}{4d} S_d \right) \Lambda^{2d-8} (u_*^{(0)})^2.
 \end{aligned}$$

*Critical exponent  $\nu$*  To determine the critical exponent  $\nu$ , we need to linearize the flow about the fixed point and determine the eigenvalue  $\lambda_r$  in the direction of the

parameter  $r$ . We have the general form of the flow equation

$$\ell \frac{d}{d\ell} \begin{pmatrix} r_\ell^{(0)} \\ r_\ell^{(2)} \\ u_\ell^{(1)} \\ u_\ell^{(1)} \\ u_\ell^{(2)} \end{pmatrix} = \beta(r_\ell^{(0)}, r_\ell^{(2)}, u_\ell^{(0)}, u_\ell^{(1)}, u_\ell^{(2)}).$$

Since the influence of  $r_\ell^{(0)}$  on the flow equations of the  $u_\ell^{(n)}$  is negligible, we can also neglect all terms  $\frac{\partial \beta_{u_\ell^{(n)}}}{\partial r_\ell^{(0)}} \simeq 0$ . Linearizing the flow equation (48) with  $\delta r_\ell^{(0)} = r_\ell^{(0)} - r_*^{(0)}$ , we get

$$\begin{aligned} \ell \frac{d\delta r_\ell^{(0)}}{d\ell} &= (2-\eta) \delta r_\ell^{(0)} - 2 \cdot \frac{S_d \Lambda^d}{(2\pi)^d} \cdot \frac{6 u_*^{(0)} + 4 u_*^{(1)} \Lambda + 4 u_*^{(2)} \Lambda^2}{(r_*^{(0)} + \Lambda^2)^2} \delta r_\ell \\ &\simeq (2-\eta) \delta r_\ell^{(0)} - 2 \cdot \frac{S_d}{(2\pi)^d} \cdot (6 \Lambda^{d-4} u_*^{(0)} + 4 \Lambda^{d-3} u_*^{(1)} + 4 \Lambda^{d-2} u_*^{(2)}) \delta r_\ell \\ &\stackrel{(86),(87),(88)}{\simeq} (2-\eta) \delta r_\ell^{(0)} \\ &\quad - \frac{1}{18} (4-d-2\eta)(2(3-d)-3\eta) \left( \frac{6}{2(3-d)-3\eta} + \frac{4}{d-1} \frac{4-d-2\eta}{3-d-2\eta} \frac{S_{d-1}}{S_d} \right. \\ &\quad \left. + \frac{1}{d} \frac{(4-d-3\eta)(4-d-2\eta)}{2-d-2\eta} \right) \delta r_\ell \\ &= \lambda_r \delta r. \end{aligned}$$

The critical exponent  $\nu = \lambda_r^{-1}$  thus takes the form (65), as stated in the main text.

## 6. Bibliography

- [1] Gell-Mann M and Low F E 1954 *Phys. Rev.* **95** 1300–1312 URL <https://doi.org/10.1103/physrev.95.1300>
- [2] Amit D J 1984 *Field theory, the renormalization group, and critical phenomena* (World Scientific)
- [3] Zinn-Justin J 1996 *Quantum field theory and critical phenomena* (Clarendon Press, Oxford)
- [4] Vasiliev A 1998 *Functional Methods in Quantum Field Theory and Statistical Physics* (Gordon and Breach Science Publishers)
- [5] Kazakov D I 1988 *Theoretical and Mathematical Physics* **75** 440–442 URL <https://doi.org/10.1007/bf01017179>
- [6] Antonov N V and Kakin P I 2017 *Theoretical and Mathematical Physics* **190** 193–203 URL <https://doi.org/10.1134/s0040577917020027>
- [7] Duclut C and Delamotte B 2017 *Phys. Rev. E* **96** URL <https://doi.org/10.1103/physreve.96.012149>
- [8] Kardar M, Parisi G and Zhang Y C 1986 *Phys. Rev. Lett.* **56**(9) 889–892 URL <https://link.aps.org/doi/10.1103/PhysRevLett.56.889>
- [9] Pavlik S 1994 *Journal of Experimental and Theoretical Physics - J EXP THEOR PHYS* **79** 303–306
- [10] Antonov N V and Vasiliev A N 1995 *Zh. Éksp. Teor. Fiz.* **81**(3)
- [11] Wilson K G and Kogut J 1974 *Physics Reports* **12** 75 – 199 ISSN 0370-1573 URL <http://www.sciencedirect.com/science/article/pii/0370157374900234>
- [12] Wilson K G 1975 *Rev. Mod. Phys.* **47**(4) 773–840 URL <http://link.aps.org/doi/10.1103/RevModPhys.47.773>
- [13] Wegner F J and Houghton A 1973 *Phys. Rev. A* **8**(1) 401–412 URL <https://link.aps.org/doi/10.1103/PhysRevA.8.401>

- [14] Morris T R 1996 *Nuclear Physics B* **458** 477–503 URL [https://doi.org/10.1016/0550-3213\(95\)00541-2](https://doi.org/10.1016/0550-3213(95)00541-2)
- [15] Wetterich C 1993 *Physics Letters B* **30** 90–94 ISSN 0370-2693 URL <http://www.sciencedirect.com/science/article/pii/037026939390726X>
- [16] Kopietz P 2001 *Nuclear Physics B* **595** 493–518 URL [https://doi.org/10.1016/S0550-3213\(00\)00680-5](https://doi.org/10.1016/S0550-3213(00)00680-5)
- [17] Hasselmann N, Ledowski S and Kopietz P 2004 *Phys. Rev. A* **70** URL <https://doi.org/10.1103/physreva.70.063621>
- [18] Ledowski S, Hasselmann N and Kopietz P 2004 *Phys. Rev. A* **69** URL <https://doi.org/10.1103/physreva.69.061601>
- [19] Kühn T and Helias M 2018 *Journal of Physics A: Mathematical and Theoretical* **51** 375004 URL <http://stacks.iop.org/1751-8121/51/i=37/a=375004>
- [20] Berges J, Tetradis N and Wetterich C 2002 *Physics Reports* **363** 223–386 ISSN 0370-1573 renormalization group theory in the new millennium. URL <http://www.sciencedirect.com/science/article/pii/S0370157301000989>
- [21] Helias M and Dahmen D 2019 *arXiv* 1901.10416 [cond-mat.dis-nn]
- [22] Delamotte B 2012 An introduction to the nonperturbative renormalization group *Renormalization groups and effective field theory approaches to many-body systems* ed Janos Polonyi J S (Springer) pp 49–130
- [23] Wilson K G and Fisher M E 1972 *Physical Review Letters* **28** 240–243 URL <https://doi.org/10.1103/physrevlett.28.240>
- [24] Morris T R 1994 *International Journal of Modern Physics A* **09** 2411–2449 (Preprint <https://doi.org/10.1142/S0217751X94000972>) URL <https://doi.org/10.1142/S0217751X94000972>
- [25] Chow C and Buice M 2015 *J Math. Neurosci* **5**(8)
- [26] Hertz J A, Roudi Y and Sollich P 2017 *Journal of Physics A: Mathematical and Theoretical* **50** 033001 URL <http://stacks.iop.org/1751-8121/50/i=3/a=033001>
- [27] Lindén H, Tetzlaff T, Potjans T C, Pettersen K H, Grün S, Diesmann M and Einevoll G T 2011 *Neuron* **72** 859–872 URL <https://doi.org/10.1016/j.neuron.2011.11.006>
- [28] Beggs J M and Plenz D 2003 *J. Neurosci.* **23** 11167–11177
- [29] Roudi Y, Aurell E and Hertz J A 2009 *Front. in Comput. Neurosc.* **3** 1–15
- [30] Mora T and Bialek W 2011 *Journal of Statistical Physics* **144** 268–302 ISSN 1572-9613 URL <https://doi.org/10.1007/s10955-011-0229-4>
- [31] DiSanto S, Villegas P, Burioni R and Munoz M A 2018 *Proceedings of the National Academy of Sciences* **115** E1356–E1365 ISSN 0027-8424 (Preprint <http://www.pnas.org/content/early/2018/01/26/1712989115.full.pdf>) URL <http://www.pnas.org/content/early/2018/01/26/1712989115>
- [32] Bengio Y, Courville A and Vincent P 2013 *IEEE Transactions on Pattern Analysis and Machine Intelligence* **35** 1798–1828 URL <https://doi.org/10.1109/tpami.2013.50>
- [33] Mehta P and Schwab D J 2014 *ArXiv e-prints* (Preprint [1410.3831](https://arxiv.org/abs/1410.3831))
- [34] Goldenfeld N 1992 *Lectures on phase transitions and the renormalization group* (Reading, Massachusetts: Perseus books)